Chemical Geology 692 (2025) 122974

Contents lists available at ScienceDirect

Chemical Geology

journal homepage: www.elsevier.com/locate/chemgeo

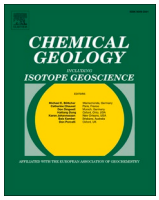

Research Paper

Paleoenvironmental evolution of the Eastern Paratethys: Tracing the Tethys Ocean legacy through geochemical proxies

Dan V. Palcu Rolier [a,b,c,*], Zhanhong Liu [d], Wei Wei [e], Sergey Popov [f], Larisa Golovina [g], Iuliana Vasiliev [h], Wout Krijgsman [b], Thomas Algeo [e,i,j]

[a] National Institute of Marine Geology and Geo-ecology, GeoEcoMar, Bucharest, Romania
[b] Fort Hoofddijk Paleomagnetic Lab, Department of Earth Sciences, Utrecht University, Netherlands
[c] Department of Geological Oceanography, Oceanographic Institute, University of São Paulo, Brazil
[d] Hubei Key Laboratory of Marine Geological Resources, College of Marine Science and Technology, China University of Geosciences, Wuhan 430074, China
[e] State Key Laboratories of Geomicrobiology and Environmental Changes (GMEC) & Geological Processes and Mineral Resources (GPMR), China University of Geosciences, Wuhan 430074, China
[f] Geological Institute, Russian Academy of Sciences, Pyzhevskiy per. 7, Moscow 119017, Russia
[g] Borissiak Paleontological Institute, Russian Academy of Sciences, Profsoyuznaya ul. 123, Moscow 117997, Russia
[h] Senckenberg Biodiversity and Climate Research Centre (SBiK-F), Frankfurt am Main, Germany
[i] Department of Geosciences, University of Cincinnati, Cincinnati, OH 45221, USA
[j] State Key Laboratory of Oil and Gas Reservoir Geology and Exploitation & Institute of Sedimentary Geology, Chengdu University of Technology, Chengdu 610059, China

ARTICLE INFO

Editor: Dr. Karen Johannesson

Keywords:
Redox
Oligocene
Miocene
B/Ga
Sr/Ba
Black Sea

ABSTRACT

During the Oligocene to Miocene, the Paratethys Sea emerged as the northern offshoot of the Tethys Ocean, separated from the Mediterranean by the Alpine-Himalayan mountain range. Its history was characterized by the opening, restriction and closure of marine gateways, resulting in significant paleoenvironmental changes, including episodes of anoxia and extreme salinity fluctuations. This study investigates the paleoenvironmental evolution of the Paratethys Sea by focusing on variations in salinity and paleoventilation through advanced geochemical analyses of key sections (Belaya, Panagia, Zhelezhny Rog) in the northern Caucasus and Taman Peninsula of Russia, spanning 42 to 4 Ma. We apply a suite of geochemical proxies to reconstruct paleosalinity [e.g., using the boron/gallium (B/Ga), strontium/barium (Sr/Ba), sulfur/total organic carbon (S/TOC) ratios] and paleoredox conditions [e.g., using the organic carbon/phosphorus (C_{org}/P) ratio as well as trace-metal enrichment factors such as Zn_{EF}, V_{EF}, and Mo_{EF}]. Our results indicate that Paratethys was influenced by both global and local events, with regional factors becoming increasingly significant as isolation and fragmentation progressed. Paleoventilation proxies reveal two main episodes of anoxia: the Kuma Anoxic Event, a regional event exhibiting oceanic anoxic signatures that encompassed the time of the Middle Eocene Climatic Optimum (MECO) and; the Maikop Persistent Basin Water Stratification (PBWS) event, coinciding with the Eocene-Oligocene Transition (EOT) and lasting until the Middle Miocene Climatic Optimum (MMCO), reflecting characteristics of an enclosed sea; and a weaker, less stable suboxic-anoxic episode in the late Miocene, associated with Megalake Paratethys. Paleosalinity proxies depict both transitions from marine to brackish conditions, such as the late Maikop salinity decrease and significant short-lived marine episodes, such as the MMCO-related mid-Langhian flood (14.8 Ma), the Badenian-Sarmatian Extinction Event (12.65 Ma) and the Intra-Maeotian Event (6.8 Ma). These findings emphasize the critical role of marine connectivity as a trigger of salinity and ventilation changes in the Eastern Paratethys's evolution, laying the groundwork for future studies on restricted basins.

* Corresponding author at: National Institute of Marine Geology and Geo-ecology, GeoEcoMar, Bucharest, Romania.
E-mail addresses: D.v.palcu@uu.nl, dan.palcu@gmail.com (D.V. Palcu Rolier).

https://doi.org/10.1016/j.chemgeo.2025.122974
Received 27 February 2025; Received in revised form 29 June 2025; Accepted 16 July 2025
Available online 18 July 2025

1. Introduction

1.1. Overview of the Paratethys realm

The Paratethys represents a pivotal and dynamic region in Eurasian paleogeography, where fragments of the ancient Tethys Ocean became progressively isolated from the global ocean during the Oligocene (Rögl and Steininger, 1983). Shaped by tectonic forces (Schmid et al., 2008), this region evolved into a complex system of semi-enclosed marine basins and epicontinental seas and lakes. It was marked by episodic disconnections and reconnections with the open ocean, triggered by a complex interplay of tectonic activity and global eustatic fluctuations (Palcu and Krijgsman, 2023), which profoundly influenced the region's hydrology, sedimentation patterns and ecosystems.

The Paratethys Realm comprised two major components: regions with more active tectonic deformation and regions characterized by relatively lower tectonic activity (Fig. 1). The tectonically active areas hosted most of the marine connections between the Paratethys and the global ocean (Palcu et al., 2023). These included the Alpine Foredeep basin, corresponding to the Western Paratethys (Sant et al., 2017), the Carpathian region (Central Paratethys; Popov et al., 2004; Kováč et al., 2017) and a series of smaller, structurally complex basins across the Balkans, Anatolia and Iran. In contrast, parts of the Eastern Paratethys, particularly those overlapping the stable Russian Platform, were less affected by major tectonic deformation. These regions had fewer, shorter-lived marine connections to the global ocean and their sedimentary basins experienced relatively continuous subsidence and deposition over extended periods. The depositional environments of the Eastern Paratethys were nevertheless influenced by nearby tectonically active regions, as the critical gateways modulating marine connectivity were primarily located in the Central Paratethys (Popov et al., 2022; Palcu and Krijgsman, 2023).

The interplay between these two Paratethys domains resulted in a series of complex paleogeographic transformations (Palcu et al., 2023) and a variable history of environmental and hydrological conditions (Fig. 2), making the Paratethys a key subject for understanding the interactions between tectonics, oceanography and paleoclimate. Due to its tectonic stability, the Eastern Paratethys is particularly informative, hosting near-continuous sedimentary successions that cover its entire Cenozoic evolution.

1.2. Importance of salinity variation in Paratethys history

Salinity and ventilation variations played a crucial role in shaping the paleoenvironmental evolution of the Eastern Paratethys (Popov et al., 2016; Simon et al., 2019). These salinity fluctuations alternated between fully marine, stratified semi-marine and brackish, while the paleoventilation shifted from oxic to suboxic or anoxic leaving a distinct and dynamic imprint on the basin's depositional history. During periods of enhanced marine connectivity, the Eastern Paratethys supported diverse faunal communities comparable to those found in modern open-ocean ecosystems (Nevesskaya et al., 2005; Popov et al., 2023; Radionova and Golovina, 2011). While classical oceanic marker species such as planktonic foraminifera and calcareous nannoplankton are often underrepresented in the fossil record of Paratethys, this may be primarily due to poor preservation in deep-water, anoxic settings. In these

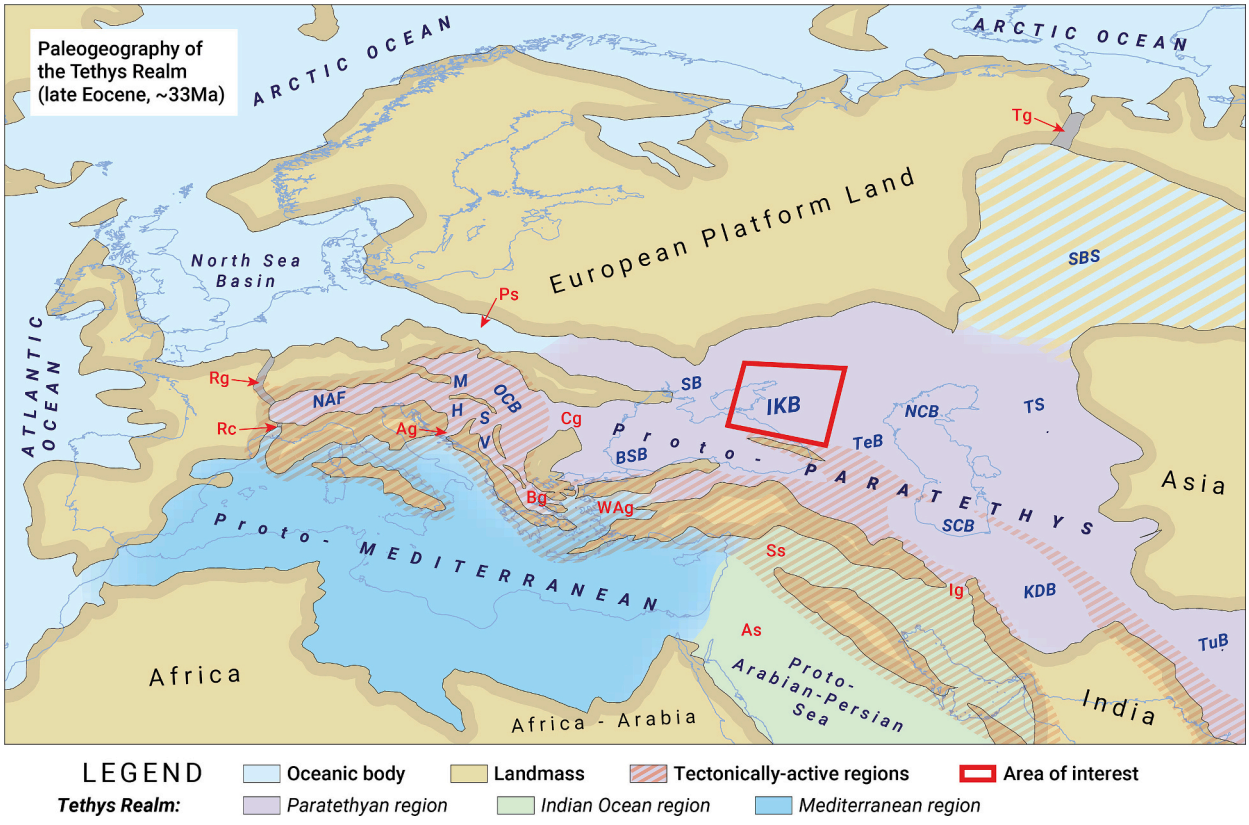

Fig. 1. Paleogeography of the Tethys realm on the eve of its demise (Eocene). Note the fragmented character of the northern realms (future Paratethys) when compared with the more homogeneous southern realm (future Mediterranean). Key basins of the future Paratethys Realm include (in blue lettering): BSB - Black Sea Basin, H - Hungarian Basin, IKB – Indol-Kuban Basin, KDB - Kopet Dagh Basin, M - Magura Sea, NAF – North Alpine Foredeep basin, NCB – North Caspian Basin, OCB - Outer Carpathian Basin, S - Szolnok Basin, SB - Scythian Basin, SBS - Siberian Sea, SCB – South Caspian Basin, TuB - Tarim Basin, TeB - Terek Basin, TS - Turan Sea, V - Vardar Trough. Connections with the global ocean (in red): Ag - Adria Gap, WAg – West Anatolian Gateway, As - Arabian Seaway, Bg - Balkan Gateway, Cg - Carasu Gateway, Ig - Iranian Gateway, Ps - Polish-Danish Strait, Rc - Rhone Corridor, Rg - Rhine Graben, Ss - Sivas Strait, Tg - Turgai Gateway. (For interpretation of the references to colour in this figure legend, the reader is referred to the web version of this article.)

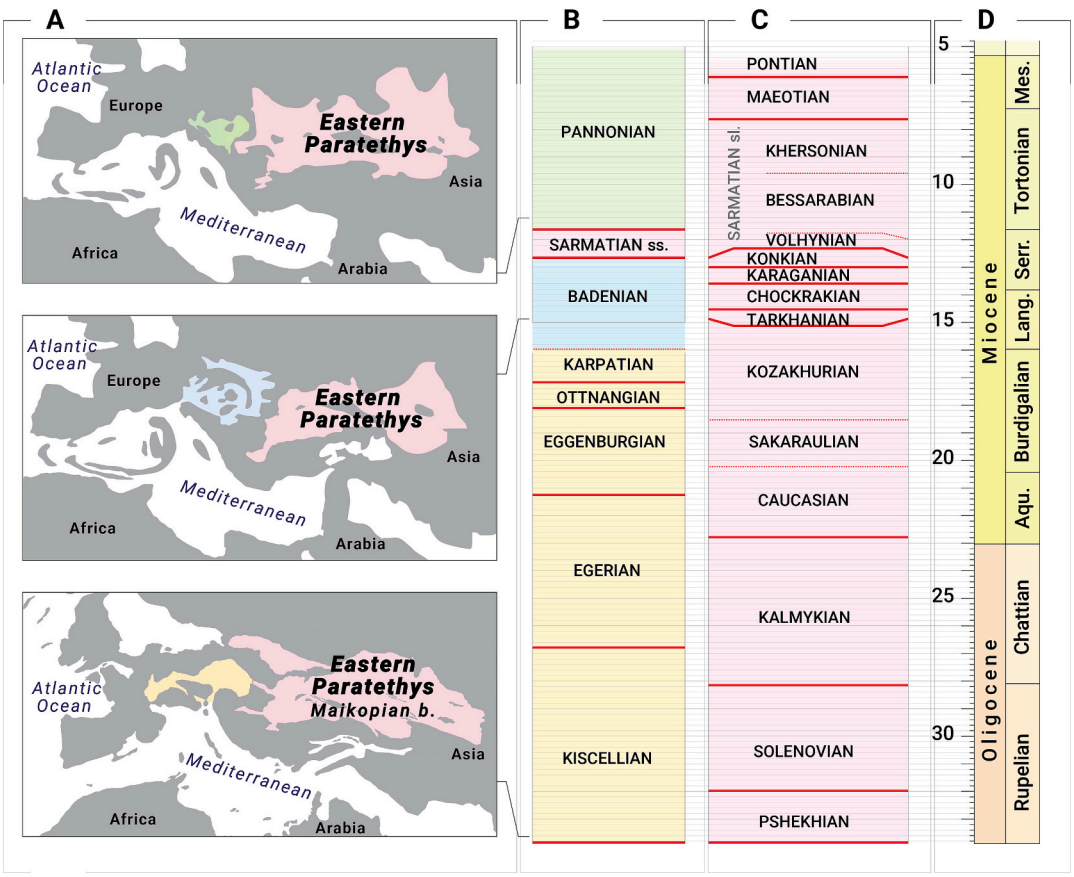

Fig. 2. Schematic paleogeographic evolution and regional stratigraphy of the Paratethys realm. (A) Simplified paleogeographic maps showing the spatial evolution of the Paratethys during key time intervals (modified after Palcu et al., 2023); (B) Regional stratigraphy of the Central Paratethys (Carpathian, Pannonian, and North Alpine regions), based on the stage definitions of Piller et al. (2007) and Kováč et al. (2017); (C) Regional stratigraphy of the Eastern Paratethys (Black Sea–Caspian Sea region), based on Popov et al. (2004, 2022); (D) Global chronostratigraphic reference frame, following the time scale of Raffi et al. (2020).

environments, early diagenetic dissolution—linked to a shallow carbonate compensation depth (CCD) and chemocline positioning—resulted in the loss of calcareous microfossils (see Soták, 2010). As such, their absence does not necessarily indicate ecological isolation from the open ocean.

Geographic isolation and restricted hydrological exchange often led to prolonged stratification and significant ecological transformations (Palcu et al., 2019a; Popov and Studencka, 2015; Soták, 2010). In these isolated settings, endemic and euryhaline species, genera and sometimes families which are adapted to brackish and highly variable salinity conditions, flourished (Nevesskaya et al., 1986, 1997, 2001; Sachsenhofer et al., 2017). At the same time, prolonged anoxia facilitated the deposition of organic-rich sediments, such as those of the Maikop Series (Gavrilov et al., 2021; van der Boon et al., 2019; Popov et al., 2008; Akhmetiev et al., 1995), which are renowned for their role in organic carbon sequestration during the Oligocene-Miocene (Allen and Armstrong, 2008).

Despite their significance, these organic-rich sediments present unique challenges. Complete absence of benthic life in anoxic conditions and dissolution of carbonate plankton (Beniamovski et al., 2003; Popov et al., 2008; Popov et al., 1993) has frequently resulted in the absence of fossils in many deposits. This lack of well-preserved biotic markers has hindered biostratigraphic correlations with global ocean records and limited paleoenvironmental reconstructions (Beniamovski et al., 2003; Popov et al., 2023; Popov et al., 1993; Jones and Simmons, 1997). Consequently, these challenges obscure a full understanding of the Eastern Paratethys' evolution and its relationship with global climatic and oceanographic events (Gavrilov and Kopaevich, 1996; Palcu and Krijgsman, 2023).

Additionally, whilst insight into salinity and ventilation are critical to interpreting the basin's paleoenvironmental dynamics, the scarcity of preserved fossils, combined with the region's complex hydrological history, limits our ability to use traditional methods to quantify these processes. Advanced geochemical analyses and innovative sedimentological approaches are essential to bridge these gaps. Such efforts will provide valuable insights into the Eastern Paratethys' role in shaping Earth's paleoenvironmental and geochemical history, revealing its contributions to global biogeochemical cycles.

1.3. Study objectives

Traditional methods for reconstructing Paratethys salinity history are based on the composition of fossil fauna and phytoplankton and their comparison with modern analogues, for which the ecological parameters are well known (Nevesskaya et al., 2005; Nevesskaya et al., 1986; Popov et al., 2023; Popov et al., 1993). While these methods provide valuable insights, their utility is constrained by the basin's endemic biota, taphonomic biases and diagenetic overprinting. These limitations necessitate the use of more robust quantitative tools. Recent advances in geochemical techniques offer a promising pathway to address these challenges. Elemental proxies, such as boron/gallium (B/Ga), strontium/barium (Sr/Ba) and sulfur/total organic carbon (S/TOC) ratios, have proven effective for reconstructing paleosalinity and paleoventilation in fine-grained siliciclastic systems (Tribovillard et al., 2006; Wei and Algeo, 2020). These proxies allow differentiation between marine, brackish and freshwater conditions, providing a quantitative framework to investigate the basin's hydrological and geochemical evolution.

This study aims to elucidate the paleoenvironmental evolution of the Eastern Paratethys by employing advanced geochemical proxies to quantify salinity fluctuations and associated ecological dynamics within sedimentary sections, located in the Northern Caucasus and Taman Peninsula, of the West Kuban Basin (Fig. 3). Specifically, the objectives of this research are threefold: (1) To employ the B/Ga, Sr/Ba and S/TOC ratios as elemental proxies to reconstruct paleosalinity variation from the Eocene to Pliocene, thereby enhancing our understanding of hydrological changes and marine connectivity within the basin. (2) To analyze spatial and temporal patterns of salinity, identifying key intervals of marine influx and freshwater input, particularly during critical phases of Paratethys history, such as the transition from the Maikop Persistent Basin Water Stratification (PBWS) event to periods of improved marine connectivity, as indicated by the elemental proxies. (3) To compare the results derived from these geochemical analyses with existing paleontological and lithological records, facilitating a comprehensive interpretation of the basin's paleoenvironmental dynamics and elucidating the mechanisms underlying the paleogeographic transformations that characterized the Eastern Paratethys throughout its history.

2. Paleoenvironmental reconstructions

2.1. Paleosalinity proxies

The boron-to-gallium ratio (B/Ga) is an effective paleosalinity proxy based on boron's adsorption onto clay minerals (Wei and Algeo, 2020). Empirical B/Ga thresholds of <3, 3–6 and > 6 classify depositional environments into freshwater (<1 psu), brackish (1–30 psu) and marine salinity facies (30–40 psu; psu = practical salinity unit). Given the broad range of salinities associated with the brackish facies, it is useful to distinguish "low-brackish" conditions (c. 1–15 psu) from "high-brackish" conditions (c. 15–30 psu; Algeo et al., 2025). A new proxy, "excess boron" (B_{xs}), can assist in the evaluation of salinity in carbonate sediments, with negative (depleted) B_{xs} values indicative of brackish conditions and values of c. 5–20 ppm of marine conditions (Wei et al., 2025). This proxy is demonstrably useful in reconstructing salinity variation in mixed shale-carbonate successions (e.g., Algeo et al., 2025) and estuaries (e.g., Zhang et al., 2025).

The strontium-to-barium ratio (Sr/Ba) leverages the distinct solubility behavior of these elements in freshwater versus marine systems. Initially developed in marine geochemical studies (Palmer and Edmond, 1989) and further adapted for sedimentary environments (McLennan, 2001), this proxy has become a widely used indicator of paleosalinity in mixed siliciclastic systems. The strontium-to-barium ratio (Sr/Ba) leverages the distinct solubility of Sr and Ba in freshwater and marine systems, with thresholds of <0.2 for freshwater, 0.2–0.5 for brackish and > 0.5 for marine conditions (Wei and Algeo, 2020). It is particularly useful for reconstructing environments characterized by freshwater–marine mixing, such as estuaries. Peaks in Sr/Ba align with marine transgressions, while low values highlight freshwater dominance during basin isolation. Ba concentrations are typically low (in the few ppb range) in most aqueous systems, making it an effective proxy for shale content (Wei and Algeo, 2020), but when employing Sr/Ba as a salinity proxy, it is essential to consider the potential influence of excess Sr and Ba derived from shale formations (Liu et al., 2025). Therefore, careful consideration and, if necessary, corrections for these factors are crucial when interpreting Sr/Ba ratios in sedimentary contexts.

S/TOC ratios serve as an important proxy for assessing sulfate availability and microbial sulfate reduction in sedimentary environments. This approach builds on foundational work linking organic matter burial and sulfur diagenesis (e.g., Berner, 1980; Jørgensen, 1982; Habicht and Canfield, 1997), where the coupling of sulfate reduction and organic carbon preservation was first quantified. Values <0.1 are indicative of freshwater conditions, while values >0.1 are associated with brackish or marine environments, as refined in modern geochemical studies (Wei and Algeo, 2020). Elevated S/TOC ratios in organic-rich sediments suggest that sulfate reduction plays a crucial role in the

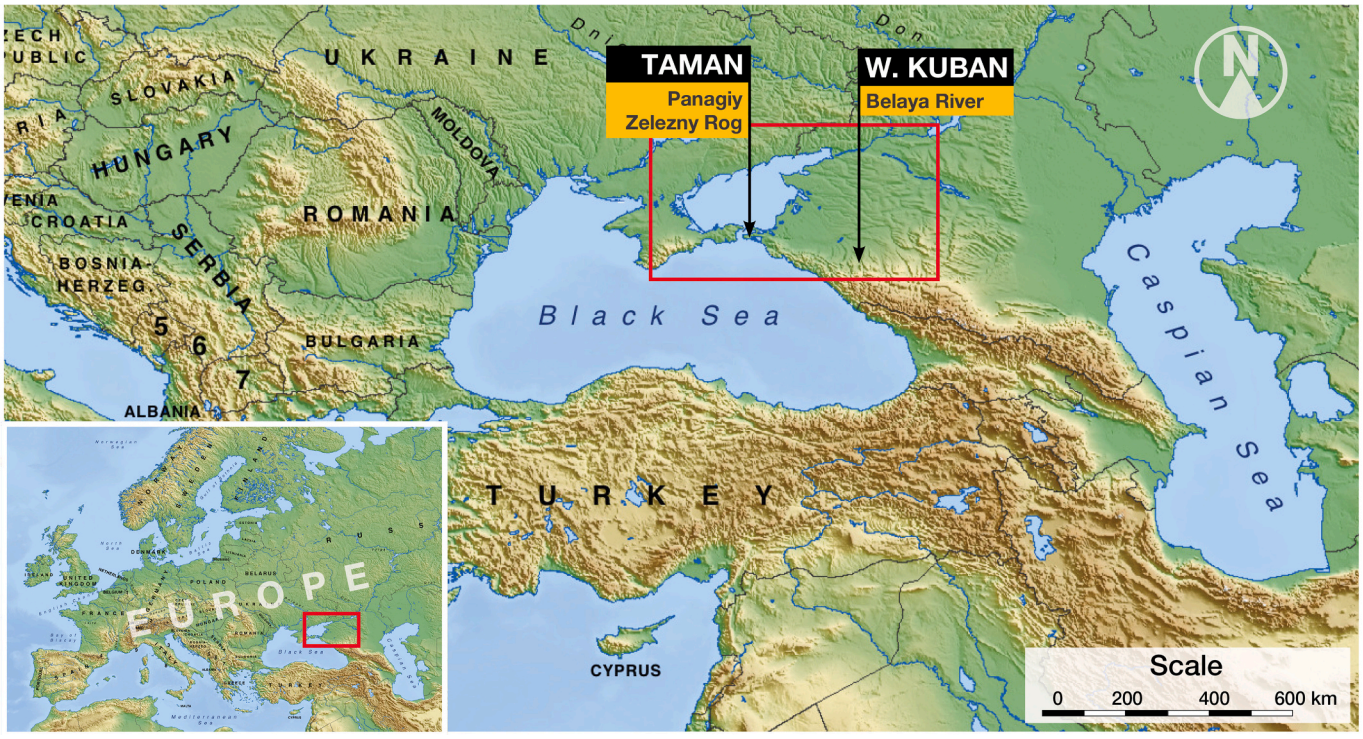

Fig. 3. Sampling locations in the Eastern Paratethys region. The Belaya section in the West Kuban Basin (van der Boon et al., 2019; Palcu et al., 2019a) was sampled to represent the Upper Eocene to Middle Miocene interval. In the Taman Peninsula, two sections were sampled, Panagia (Palcu et al., 2021; Popov et al., 2016) and Zhelezny Rog (Popov et al., 2016; Vasiliev et al., 2011), covering the Middle Miocene to Lower Pliocene interval. These sections were chosen for their near-complete stratigraphic records.

preservation of organic matter, particularly under anoxic or stratified conditions. The S/TOC salinity proxy differs from B/Ga and Sr/Ba proxies in that it is influenced not only by salinity but also by productivity and redox processes (Wei and Algeo, 2020). The amount of organic matter present in sediment is strongly dependent on primary productivity, while the uptake of reduced sulfur is affected by both redox conditions — such as anoxia, which leads to microbial sulfate reduction — and the presence of aqueous sulfate, characteristic of non-freshwater environments. As such, the S/TOC proxy effectively distinguishes between freshwater facies (lacking aqueous sulfate) and non-freshwater facies (having aqueous sulfate) but it is not a reliable means of differentiating between brackish and marine salinity conditions (Wei and Algeo, 2020; Liu et al., 2025).

2.2. Paleoventilation proxies

Paleoventilation proxies shed light on the oxygen levels and redox conditions prevailing in a given depositional setting. We utilize the redox classification system of Algeo and Li (2020) in the following analysis. Integration of these datasets enables evaluation of joint salinity–redox dynamics in the study sections. The enrichment factors for trace metals (e.g., Zn_{EF} and V_{EF}) supplies valuable insight into paleoventilation and redox processes.

The organic carbon-to-phosphorus ratio (C_{org}/P) reflects the interplay between organic matter deposition and oxygen levels (Algeo and Ingall, 2007). Elevated ratios indicate anoxic or euxinic conditions where organic matter preservation exceeds phosphorus recycling. C_{org}/P ratios >125 are often indicative of euxinic conditions, whereas values between c. 75 and 125 may reflect dysoxic conditions (Algeo and Li, 2020). Ratios >200 are considered strong evidence for severe anoxia or euxinia, where organic matter burial outpaces phosphorus release into the water column. Lower C_{org}/P ratios, typically <75, are associated with oxic conditions, where phosphorus recycling is more efficient and organic carbon is more readily decomposed.

The zinc enrichment factor (Zn_{EF}) quantifies zinc retention in euxinic environments, often correlating with organic substrates or sulfides (Tribovillard et al., 2006). Elevated Zn_{EF} values indicate higher productivity and the presence of euxinic conditions, thus serving as a proxy for periods characterized by increased biological activity and anoxia in the water column. In oxic marine environments, zinc primarily exists as soluble cations or complexes with organic compounds. Under reducing conditions, particularly in the bacterial sulfate reduction zone, zinc can be incorporated into sulfide minerals.

The vanadium enrichment factor (V_{EF}) acts as a sensitive marker of redox states, exhibiting enrichment in anoxic conditions due to vanadium's redox-sensitive characteristics (Tribovillard et al., 2006). Peaks in V_{EF} often coincide with euxinic episodes, marking periods of severe oxygen depletion in stratified basins and offering insight into the timing and intensity of anoxic conditions in the geological record.

The molybdenum enrichment factor (Mo_{EF}) further delineates euxinic environments, highlighting the enrichment of molybdenum through incorporation into sulfide complexes, complementing V_{EF} and C_{org}/P trends, thus refining paleoredox dynamics reconstructions (Algeo and Tribovillard, 2009). Mo_{EF} is especially useful for identifying long-term euxinic episodes and refining interpretations of ancient redox dynamics in sedimentary sequences. However, the use of Mo concentrations as proxies, requires considering factors such as basin restriction that can affect the relationship between Mo abundance and sedimentary redox dynamics (Tribovillard et al., 2006).

3. Geological context

The Kuban Basin contains one of the most extensive and continuous geological records of the ancient Paratethys Sea, spanning from the Middle Eocene to the Early Pliocene. Its central paleogeographic position within the Eastern Paratethys realm makes it a key area for reconstructing regional paleoenvironmental trends. Importantly, the basin was located on the stable Russian Platform and experienced relatively consistent subsidence with minimal tectonic disruption compared to surrounding areas (Popov et al., 2019b; Palcu et al., 2019a). This relative tectonic stability enabled long-term accumulation of fine-grained, hemipelagic sediments, which are less susceptible to local geomorphological influences. Additionally, geochemical, micropaleontological and sedimentological records from the Kuban Basin show strong correlations with other well-studied studied Paratethyan basins, such as the Caspian and Black Sea basins, reinforcing its significance as a representative archive for basin-wide environmental signals (Stoica et al., 2016; Palcu et al., 2017, 2021).

Our study concentrates on two key regions within the Kuban Basin (Fig. 3): the Pre-Caucasus, where the older portion of our stratigraphic interval is exposed. This interval is gently tilted and has been shaped by erosion from the rivers of the Caucasus, with the Belaya River Valley providing some of the most complete exposures for the Middle Eocene to Middle Miocene interval (Popov et al., 2019b,c; van der Boon et al., 2019). The younger part of the study interval is found on the Taman Peninsula, an area with a more distal position in the basin relatively undisturbed by coarse clastic sediments and continental transitions, where mud diapirs and coastal erosion provide a near-complete exposure of the Middle Miocene–Pliocene interval (Vasiliev et al., 2011; Radionova et al., 2012).

3.1. Field sites and sample collection

3.1.1. Belaya River section

The Belaya River section (N 44.366426° / E 40.196930°), located upstream of Maikop in western Ciscaucasia, is the lectostratotype of the Maikop Group (Akhmetiev et al., 1995; Grossheim, 1960; van der Boon et al., 2019; Popov et al., 2019b). This c. 1300-m-thick, well-exposed succession spans from the middle Eocene (c. 42 Ma) to the top of the middle Miocene (c. 12 Ma), corresponding to the Lutetian through Serravallian stages (Raffi et al., 2020; Speijer et al., 2020; Sachsenhofer et al., 2017; Popov et al., 2023).

At the base of the investigated interval, the Keresta Formation consists of fine-grained white marls deposited under outer shelf, carbonate-dominated conditions reflecting relatively open-marine, low-energy settings. It is overlain by the Kuma Formation (c. 45 m; late Eocene), composed of brown to dark gray, organic-rich marls deposited in deep, anoxic marine settings, indicative of low-energy, restricted basinal environments. The Belaya Glina Formation (c. 60 m; early Oligocene) follows, representing oxygenated conditions within a deep marine, low-energy depositional environment.

The Maikop Series (c. 635 m; Oligocene to early Miocene) comprises finely laminated, black shales indicative of anoxic, low-energy environments in a deep, stratified marine basin. The onset of the Tarkhanian stage (c. 14.85–14.75 Ma; Langhian, Middle Miocene) is marked by a lithologic change to carbonate clays with abundant fossiliferous content and carbonate fragments, signifying the return of ventilated marine conditions, deposited on an open shelf under moderate-energy settings. The Chokrakian (c. 14.75–13.8 Ma; Langhian) (c. 190 m) is dominated by alternations of biohermal limestones and clays, deposited in a restricted-marine shelf environment with episodic carbonate production. The overlying Karaganian (c. 13.8–13.3 Ma; Serravallian, Middle Miocene) (~185 m) features clays, silts, and thin stromatolitic limestones, indicating low-energy, marginal-marine conditions likely associated with inner shelf or lagoonal environments. The Konkian (c. 13.3–12.65 Ma; Serravallian) (c. 150 m) contains poorly cemented silts and sands reflecting shallow, nearshore deposition in higher-energy coastal settings. The Volhynian (c. 12.65–12.0 Ma; late Serravallian) is marked by thick offshore clays, signifying a return to deeper marine environments, representative of a low-energy outer shelf or upper slope setting.

3.1.2. Panagia coastal section

The Panagia section (N 45.135420° / E 36.652599°), exposed in the Black Sea cliffs near Cape Panagia (Taman Peninsula), has a thickness of c. 660 m encapsulating a largely continuous record spanning the Middle to Late Miocene (c. 13.3–6.1 Ma), encompassing the Serravallian to Messinian stages (Popov et al., 2016, 2023).

The lower part of the section corresponds to the upper part of the Konkian (c. 13.3–12.65 Ma; Serravallian), composed of dark gray, laminated clays with interbedded limestones. This reflects deepening and stagnating marine conditions within a low-energy, semi-restricted outer shelf setting. The overlying Sarmatian sensu lato (c. 12.65–7.65 Ma) straddles the Serravallian–Tortonian transition and consists of slightly calcareous clays, deposited in moderately deep, low-energy marine environments transitioning upwards into gray-green laminated clays with microbial bioherms, indicative of shallow, storm-influenced shelf settings (Palcu et al., 2021). Toward the top, interbedded clays and carbonates reflect episodic shallow-marine carbonate production, suggesting periodic shoaling in a variable marine environment. The Maeotian (c. 7.65–6.1 Ma; late Tortonian-Messinian) forms the upper part of the section (c. 20 m), dominated by calcareous clays and bryozoan reef debris, indicating a shallow marine shelf environment with localized carbonate reef development.

3.1.3. Zhelezhny Rog coastal section

The Zheleznyi Rog section (N 45.114971° / E 36.758008°) has a total thickness of c. 400 m (Fig. 4) and is located on the Black Sea coast near Zheleznyi Rog Cape. It is a key reference for the Neogene stratigraphy of the Eastern Paratethys (Krijgsman et al., 2010; Popov et al., 2023; Popov et al., 2016; Stoica et al., 2016; Popov and Zastrozhnov, 1998; Radionova et al., 2012; Vasiliev et al., 2011).

The lower portion of the succession encompasses upper Sarmatian to basal Maeotian deposits (approximately 9.8–7.65 Ma; Tortonian), characterized by clays and carbonates indicative of low-energy, basin environments, often under dysoxic bottom-water conditions in a semi-restricted setting. Overlying these, the Maeotian strata (circa 7.6–6.1 Ma; Messinian, Late Miocene) comprise dark clays, diatomaceous interbeds, and carbonate layers rich in mollusks and diatoms, reflecting fluctuating salinity, stratified water-column conditions, and transitional marine–brackish settings. A notable feature within the middle Maeotian is a ~ 15-m-thick mass transport deposit, associated with the Intra-Maeotian Event (IME), dated at 6.8 ± 0.5 Ma (Palcu et al., 2019b). This deposit is interpreted as a high-energy slope failure or gravity flow event within an otherwise stratified, low-energy basin. The IME marks a new episode in the hydrodynamic history of Paratethys, market by the episodic return of Mediterranean faunal elements in Paratethys (Golovina et al., 2019), indicative of the reconnection of Paratethys with the Mediterranean realm.

Above the IME, the Pontian stage (6.1–5.2 Ma; Messinian) is represented by alternating clays, marls, and diatomites, culminating in oolitic sands and shelly limestones. These lithologies indicate an increasingly restricted, nearshore to lagoonal setting, associated with shoaling and reduced marine connectivity. The Pontian partly overlaps with the Messinian Salinity Crisis (MSC) observed in the Mediterranean realm, suggesting a broader geodynamic influence across the Paratethys and adjacent basins (van Baak et al., 2017). The uppermost interval, assigned to the Kimmerian (c. 5.2–5.0 Ma; early Zanclean, Pliocene), consists of oolitic sands and silts, indicating the permanence of restricted, nearshore to lagoonal setting.

3.2. Age models

For the Belaya River section, we predominantly relied on the age model established by Cramwinckel et al. (2023). The age model for Lower Oligocene strata in Belaya was derived from van der Boon et al. (2019), while the Upper Oligocene to Lower Miocene age model was constructed using age constraints from Popov et al. (2019b), Filippova et al. (2015) and Golovina et al. (2024). The uppermost segment of the Belaya age model was derived from Palcu et al. (2019a).

For the Panagia coastal section on the Taman Peninsula, we employed the age models of Palcu et al. (2021, 2017). For the Zheleznyi Rog coastal section, we utilized the magnetostratigraphic and radioisotopic ages of Vasiliev et al. (2011) in conjunction with constraints derived from cyclostratigraphic analyses conducted by Rostovtseva and Rybkina (2017), Rybkina et al. (2015), and Rybkina and Rostovtseva (2014). A comprehensive overview of these combined age models is available in Supplementary Table 1.

4. Methodology

Analytical methods involved inductively coupled plasma mass spectrometry (ICP-MS) and carbon-sulfur (C—S) elemental analysis. These were performed on 192 sediment samples from the Belaya, Panagia, and Zhelezny Rog sections.

ICP-MS analyses were conducted at the State Key Laboratory for Geological Processes and Mineral Resources at China University of Geosciences, Wuhan. Samples underwent two distinct ICP-MS runs: one targeted boron and another focused on other elements, providing high-resolution isotopic data essential for determining paleosalinity proxies. Prior to trace-element analysis, c. 40 mg of sample powder were dissolved in a concentrated HF-HNO_3 mixture (15-M HF and 12-M HNO_3) in a high-pressure Teflon bomb. For boron concentration analysis, c. 40 mg of sample powder were placed in a nickel crucible and melted at c. 700 °C; the residue was then dissolved in 0.1-M HCl. Both solutions were then diluted to 50 mL with 3 % HNO_3. Results were rigorously calibrated using blanks, replicate samples, an internal laboratory standard (containing 10 mg/L of Rh) and a Chinese geological standard reference material (GSR-5; [B] = 144 ppm) to correct for potential instrument drift and to ensure data accuracy and precision, yielding analytical precisions (RSD) better than ±2 % for major elements and ± 5 % for trace elements (including B). Results for B, Ga, Sr and Ba are given in units of parts per million (ppm), and B/Ga and Sr/Ba were calculated as weight ratios.

Sulfur and carbon concentrations were measured using an Eltra 2000C—S analyzer at the Geochemistry Laboratory of the University of Cincinnati. Prior to analysis, each sample was dried and ground to a particle size of 200 mesh. A 0.1 g aliquot of the powdered sample was combusted at 1440 °C in an oxygenated atmosphere and the resulting gases were collected to determine total carbon (TC) and total sulfur (TS) content. For the determination of total organic carbon (TOC), an additional 0.1 g of sample was dissolved in 10 % hydrochloric acid and the residue was rinsed, dried and weighed before combustion in the C—S analyzer. TIC content was determined by difference (i.e., total carbon minus TOC). Data were calibrated using a two-point procedure to the USGS standard SDO-1 (C = 9.68 %, S = 5.35 %) and the Alpha Resources soil standard (C = 0.10 %, S = 0.10 %). Results are accurate to better than ±2.5 % for carbon and ± 5 % for sulfur.

5. Results

The three study sections reveal significant temporal variability in redox-sensitive trace elements, major element enrichments, and organic matter proxies between c. 41.4 Ma and 4.5 Ma. These variations reflect major paleoenvironmental changes, including shifts in oxygenation, productivity, salinity, and detrital input.

5.1. Salinity and watermass indicators

The B/Ga ratio varies between 3.4 and 9.0, with higher values (>7) in the 39–33 Ma and 26.9–24.6 Ma intervals (Fig. 5a). These peaks align temporally with Mo and V enrichments. B and Ga individual concentrations show correlation with B/Ga, suggesting that both boron enrichment and Ga dilution may influence the salinity proxy. A shift toward lower B/Ga and decreasing B concentrations occurs after c. 24.6

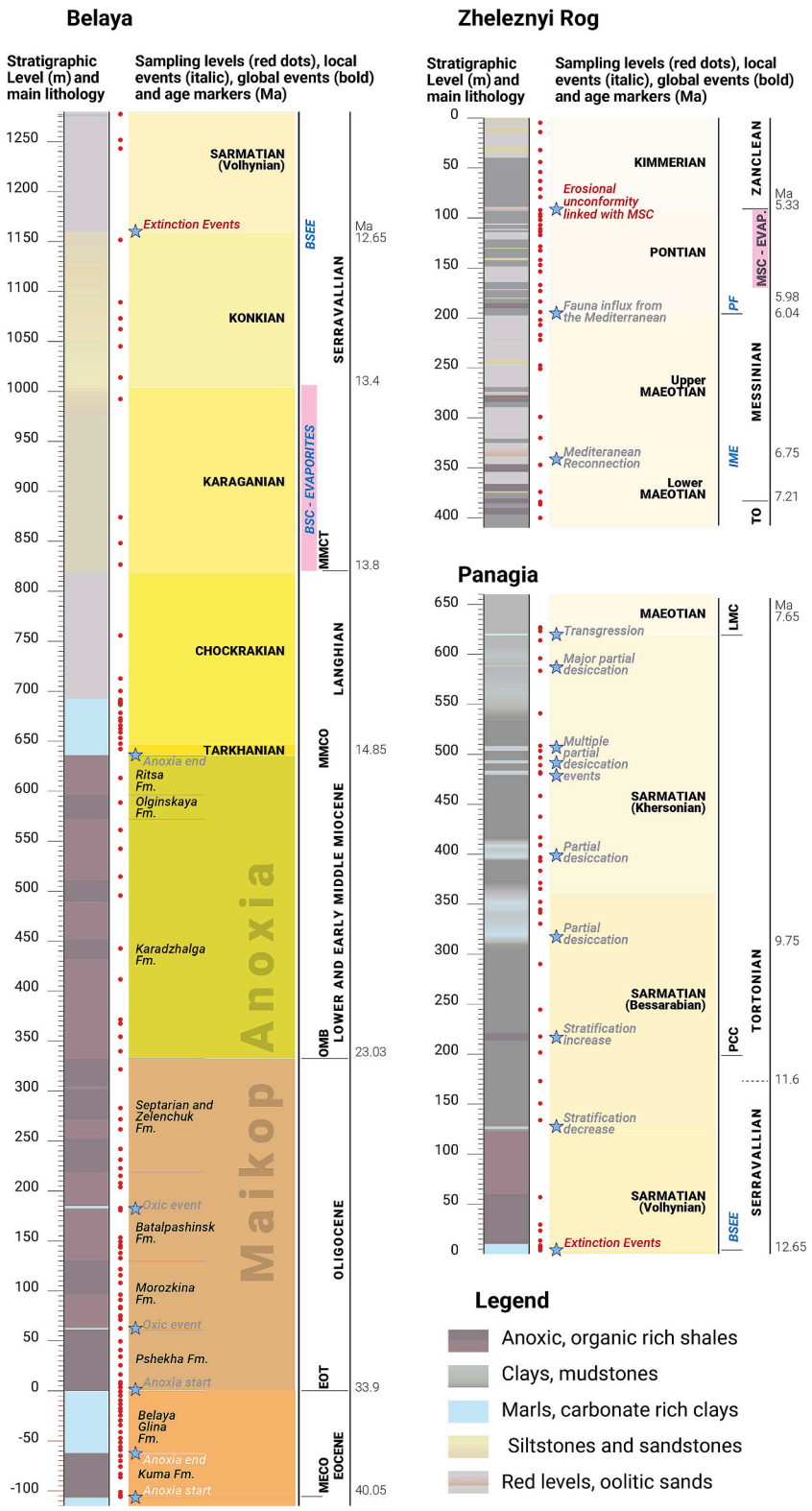

Fig. 4. Lithological columns of the sections analyzed, incorporating a suite of integrated age models based on a synthesis of independent studies using biostratigraphy, magnetostratigraphy, tephrostratigraphy, and cyclostratigraphy. Key paleoenvironmental and climatic events are labeled as follows: MECO – Middle Eocene Climatic Optimum, EOT – Eocene-Oligocene Transition, OMB – Oligocene-Miocene Boundary, MMCO – Middle Miocene Climatic Optimum, MMC – Middle Miocene Cooling, BSC – Badenian Salinity Crisis, BSEE – Badenian–Sarmatian Extinction Event, KVT – Konkian–Volhynian Transition, PCC – Pacific Carbonate Crush, LMC – Late Miocene Cooling, TMB – Tortonian–Messinian boundary, IME – Intra–Maeotian Event, MSC – Messinian Salinity Crisis, ZF – Zanclean Flooding. Blue stars indicate events discussed in the manuscript. Additional context and references for the sections, events, and age models are provided in the corresponding text sections. (For interpretation of the references to colour in this figure legend, the reader is referred to the web version of this article.)

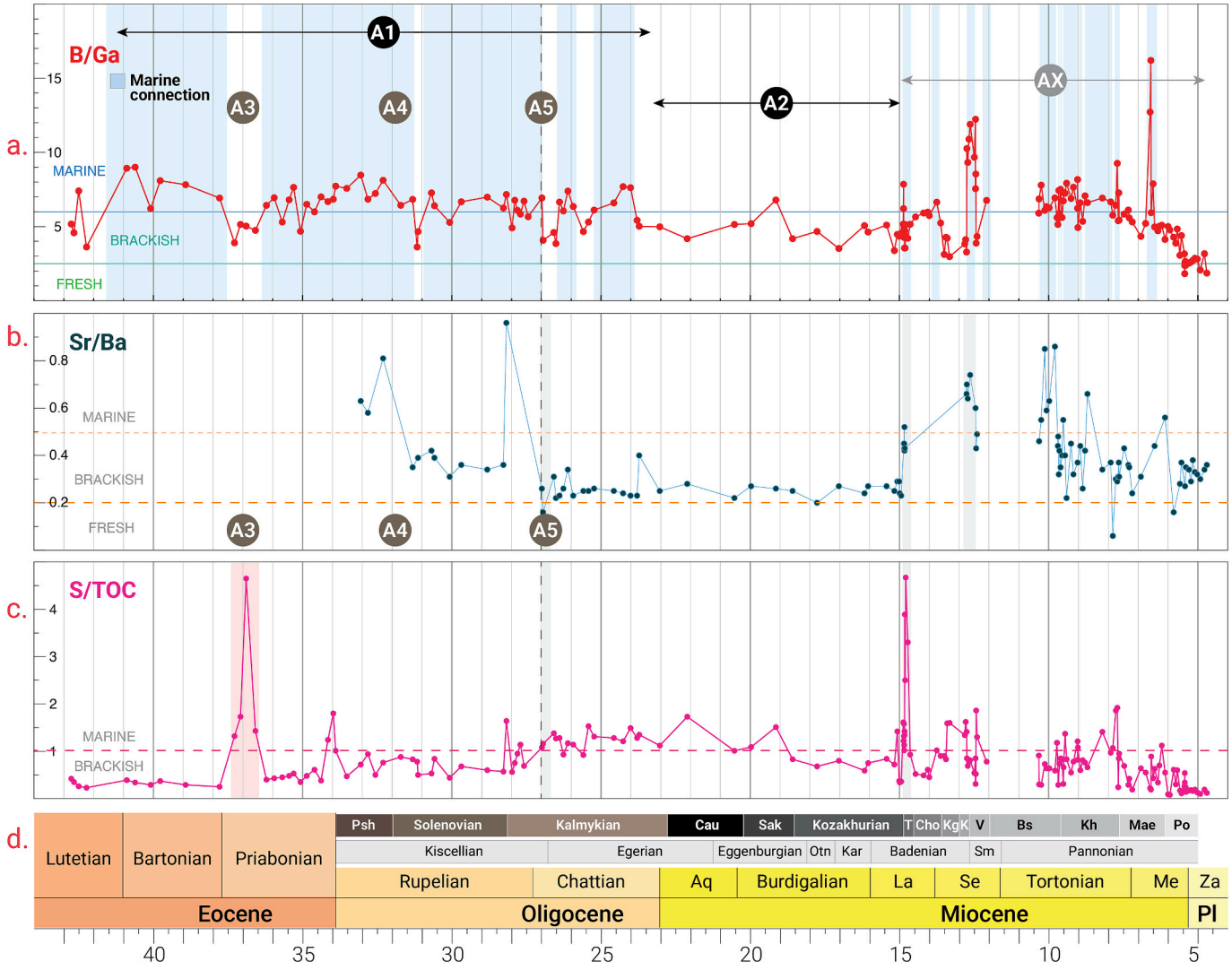

Fig. 5. Paleoenvironmental history of Eastern Paratethys: paleosalinity and paleoproductivity. Black circles (A1-A2) represent main phases, dark brown circles represent major events (A3-A5) and gray circles represent other events or regional events (AX); **(a)** B/Ga; **(b)** Sr/Ba; **(c)** S/TOC; **(d)** Timescale of Eastern Paratethys regional stages, Central Paratethys regional stages and global stratigraphic units (Raffi et al., 2020); Acronyms for stages (St.) and substages (Sb.) in Eastern Paratethys regional (Russian) stratigraphy: Psh – Pshekhian St., Cau – Caucasian St., Sak – Sakaraulian St., T – Tarkhanian St., Cho – Chockrakian St., Kg – Karaganian St., K – Konkian St., V – Volhynian Sb., Bs – Bessarabian Sb., Kh – Khersonian Sb., Mae – Maeotian St., Po – Pontian St., Acronyms in Central Paratethys stratigraphy: Otn – Ottnangian St., Kar – Karpatian St., Sm – Sarmatian St., Acronyms in global stratigraphy: Aq – Aquitanian St., La – Langhian St., Se – Serravallian St., Me – Messinian St., Za – Zanclean St., Pl – Pliocene Epoch. Discriminatory cutoff values are discussed in the text. (For interpretation of the references to colour in this figure legend, the reader is referred to the web version of this article.)

Ma.

The Sr/Ba ratio shows considerable variability throughout the record (Fig. 5b). Values range from as low as 0.06 to 1.32. A notable peak of Sr/Ba = 1.32 is observed at 37.30 Ma, concurrent with high S/TOC (1.73) and elevated Mo_{EF}. From c. 33 to 25 Ma, Sr/Ba fluctuates between 0.2 and 0.8. Between 15 and 5 Ma, Sr/Ba values remain relatively stable (c. 0.2–0.6), with minor local enrichments (e.g., Sr/Ba = 0.85 at 10.13 Ma or 0.86 at 9.79 Ma).

The S/TOC ratio ranges from 0.08 to 4.67 through the composite section (Fig. 5c). Elevated S/TOC ratios >1.0 are most prominent in three key intervals: 37.3–36.6 Ma, peaking at 4.65 at 36.89 Ma; 26.2–23.2 Ma, where values persistently remain >1.0 (e.g., 1.49 at 23.44 Ma), aligning with high Mo_{EF} and C_{org}/P ratios; 14.8–13.3 Ma, with a distinct maximum of 4.67 at 14.78 Ma. In contrast, S/TOC <0.5 dominates the youngest part of the record (after c. 12 Ma),

5.2. Redox proxies and trace-element concentrations and enrichment factors

C_{org}/P ratios are particularly elevated in the c. 41.2 to c. 37.5 Ma interval (Fig. 6a), reaching maximum values above 350 (e.g., 356 at 37.54 Ma). The rise in sulfur content (S > 1 wt%) is synchronous with Mo_{EF} (>20). From c. 37.3 Ma onward, C_{org}/P ratios sharply decline, stabilizing below 50, with intermittent pulses of enrichment (e.g., 202 at 26.16 Ma). The relatively stable S content from c. 36 to 26 Ma (0.1–0.9 wt%) suggests a shift toward less sulfidic environments.

Zinc (Zn) concentrations and Zn_{EF} exhibit lower variability, with Zn ranging from c. 25 to 226 ppm and Zn_{EF} between 0.96 and 9.35 (Fig. 6b). Zn_{EF} values peak around c. 36.08 Ma, coeval with Mo enrichment.

Vanadium (V) concentrations range from 41 to 625 ppm, with V_{EF} values spanning 1.3 to 11.5 (Fig. 6c). A marked increase in V and V_{EF} is observed from c. 41.2 Ma (V = 65 ppm; V_{EF} = 3.3) to a peak at c. 38.0 Ma (V = 625 ppm; V_{EF} = 11.5). After this interval, both parameters gradually decrease, stabilizing around V_{EF} c. 1.5 by c. 23 Ma.

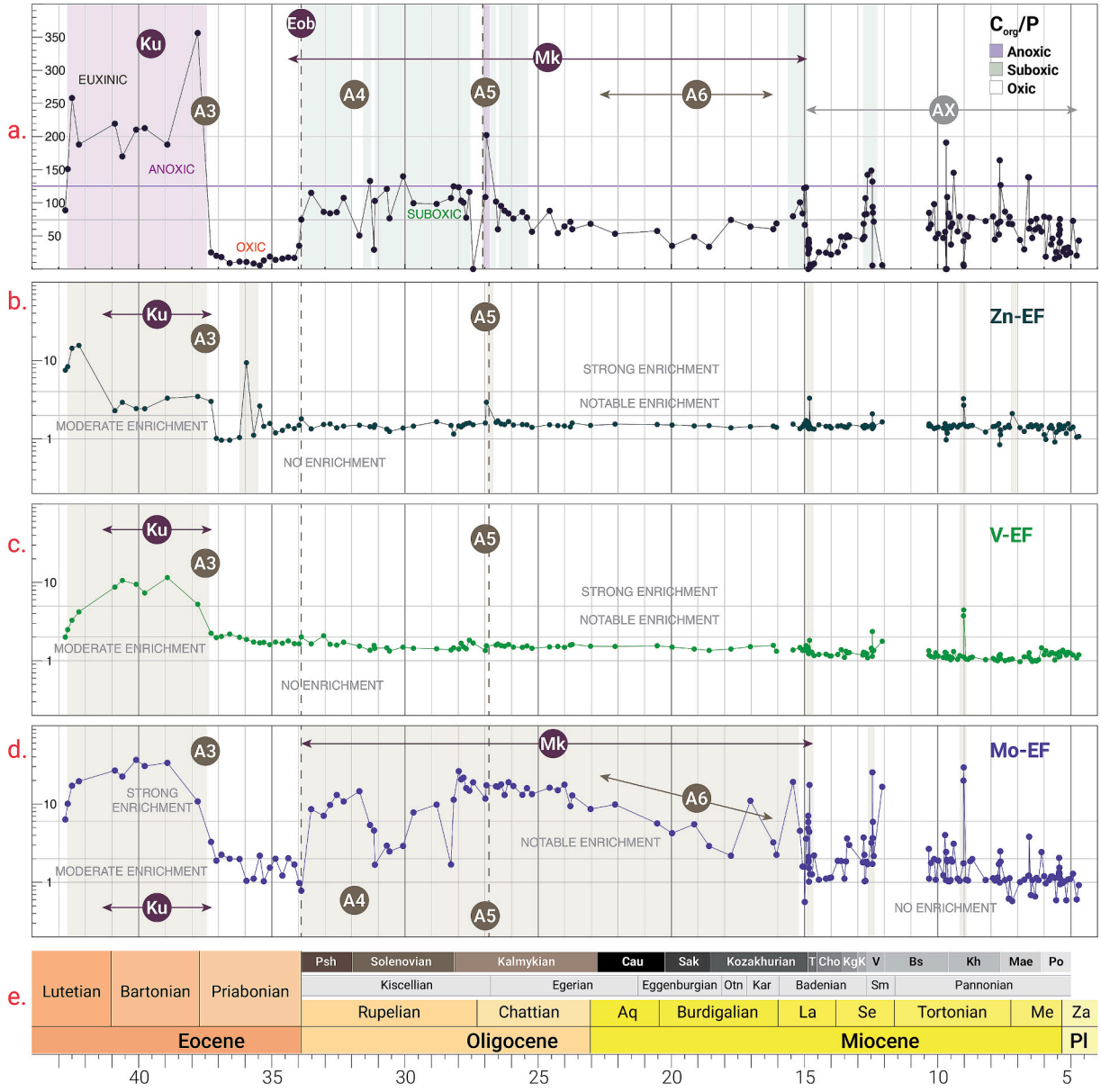

Fig. 6. Paleoenvironmental history of Eastern Paratethys: paleoventilation. Dark brown circles represent events (A3-A6), purple circles represent anoxic phases (e.g., Ku) and gray circles represent other events or regional events (AX). **(a)** The C_{org}/P proxy records an anoxic interval corresponding to the Kuma Anoxic Event (Ku) the post-Kuma oxic recovery (A3) and the Maikop PBWS event (Mk). The Maikop interval is documented by suboxic values throughout the Oligocene, followed by gradual oxygenation in the Lower Miocene (A6) and a phase of paleoventilation instability in the Upper Miocene (AX). **(b-c)** Zinc (Zn_{EF}) and vanadium (V_{EF}) enrichment factors imply strong enrichment during the Kuma Anoxic Event but only moderate enrichment during the Maikop PBWS event. **(d)** Mo enrichment factors (Mo_{EF}) match the C_{org}/P proxy trends and events with strong enrichment values during both the Kuma and Maikop. **(e)** Timescale showing the Eastern Paratethys regional stages, Central Paratethys regional stages and Global Stratigraphic units (Raffi et al., 2020). See Fig. 5 for abbreviations. (For interpretation of the references to colour in this figure legend, the reader is referred to the web version of this article.)

Molybdenum (Mo) concentrations are similarly variable, with Mo ranging from <1 to 67.7 ppm and Mo_{EF} reaching a maximum of c. 67.7 at c. 38.9 Ma (Fig. 6d). The most intense Mo enrichments ($Mo_{EF} > 30$) occur between c. 39 and 26.5 Ma. A distinct Mo_{EF} peak of 45.17 occurs at 39.76 Ma, synchronized with high C_{org}/P and S content.

6. Discussion

Initial scenarios outlining Paratethys's paleoenvironmental evolution were primarily derived from paleontological and lithological data accumulated over more than 150 years across the entire basin (see Popov et al., 2019a, 2022). In order to assess the significance of our new elemental compositions and geochemical indices it is essential to correlate these with biotic data. Our findings align well with the documented history of the Paratethys, uncovering distinct trends and transformations over time.

6.1. Prelude to Paratethys (Middle Eocene – terminal Eocene, 42–34 Ma)

Geochemical data from the Eastern Paratethys indicate that the Middle to Late Eocene interval (42–34 Ma) marks a key transition in the basin's paleoenvironmental evolution. B/Ga values from the lower part of the succession plot within the marine range, supporting the interpretation of open ocean connectivity during the early part of this interval (Fig. 5, A1). However, B/Ga values decrease markedly within carbonate-rich intervals, particularly in the late Eocene, where they fall

within the brackish range. This apparent contradiction with extensive faunal evidence for fully marine conditions (e.g., cosmopolitan foraminifera, plankton-rich marls) suggests that lithological controls, rather than true salinity variation, dominate the geochemical signal. Specifically, in carbonate-dominated sediments, low clay content reduces the capacity for boron incorporation, leading to systematic underestimation of paleosalinity (Wei and Algeo, 2020; Liu et al., 2024). This effect is further supported by the poor performance of the S/TOC proxy in the same intervals, with generally low values except in select carbonate-rich layers. The Sr/Ba proxy is not interpretable in these settings due to elevated bulk Sr concentrations, likely tied to carbonate mineralogy, which suppresses the sensitivity of the ratio to salinity gradients.

In contrast to the paleosalinity proxies, redox proxies yield a more consistent picture. The C_{org}/P ratio identifies a clear interval of bottom-water anoxia spanning the middle to late Eocene, coinciding with the stratigraphic extent of the Kuma Formation (Fig. 6a). This anoxic signal is substantiated by elevated enrichment factors for redox-sensitive trace elements, including Mo_{EF}, V_{EF}, and Zn_{EF} (Fig. 6b–d). These geochemical signatures are consistent with the widespread deposition of organic-rich mudstones characteristic of the Kuma Formation, which is known from multiple localities across the Eastern Paratethys (Beniamovski et al., 2003; Gavrilov et al., 2000; Zaporozhets, 1999; Popov et al., 2019c). Taken together, these data confirm the presence of a persistent and regionally extensive anoxic event—the Kuma Anoxic Event—that defined the proto-Paratethys hydrology during the late Eocene.

This geochemical evidence aligns with broader paleogeographic and tectonic reconstructions. During the Paleogene, the Tethys Ocean formed a broad marine corridor between Africa and Eurasia, with connections to the North Atlantic via the Pre-Alpine and Pre-Carpathian troughs (Kaya et al., 2019). Around 42 Ma, the initial collision between the Arabian and Eurasian plates triggered regional tectonic reorganization (Darin et al., 2018), accompanied by widespread volcanism in the Pontides (Schleiffarth et al., 2018; Okay et al., 2022) and a volcanic flare-up along the Neotethys subduction zone (van der Boon et al., 2021). This magmatic episode, active between ~44 and 37 Ma, overlaps with the timing of the Kuma Anoxic Event (41.4–37.4 Ma), and contributed to the growing oceanographic isolation of the Peri-Tethys. Volcanic emissions, especially from magma-carbonate interaction, may have added substantial CO_2 to the ocean–atmosphere system, fostering greenhouse warming, stratification, and redox instability. Although a direct causal link remains uncertain, the flare-up likely acted as a background driver of anoxia. These processes, along with narrowing marine gateways, promoted enhanced vertical stratification within the Eastern Paratethys, thereby limiting bottom-water ventilation (Palcu and Krijgsman, 2023). Although the Middle Eocene Climatic Optimum (MECO; ~40.5–40.0 Ma) has been proposed as a potential trigger for anoxia (Bohaty and Zachos, 2003), the onset of Kuma predates MECO, and anoxia persisted well beyond its ~500 kyr duration (Cramwinckel et al., 2023). Our data suggest that sustained tectonic restriction and broader geodynamic forcing were primary controls on Eocene deep-water oxygenation.

The late Eocene also witnessed a partial reorganization of the basin. By ~38.4 Ma, geochemical and lithological changes indicate improved oxygenation and increased faunal diversity, marking a transition from anoxic to more ventilated conditions (Fig. 6a, A3). This corresponds to the deposition of the Belaya Glina Formation—widespread marl sequences rich in bioturbation, plankton, and cosmopolitan warm-water foraminifera (Gavrilov et al., 2017; Musatov and Bogachkin, 2019). The establishment of this carbonate factory reflects enhanced watermass exchange and likely signals a temporary re-establishment of open-marine conditions in the waning stages of the Eocene.

Overall, the geochemical record confirms that the Eastern Paratethys underwent major hydrological and redox transformations during the Eocene. This period marks the initiation of *pre*–Paratethys basin restriction, with the development of strong water-column stratification, bottom-water anoxia, and reduced exchange with the global ocean. These conditions foreshadowed the isolation trends that would later dominate the Neogene history of the Paratethys and contributed to the early evolution of endemic environmental and biotic regimes.

6.2. Anoxic marine phase (Oligocene–Middle Miocene, 34–15 Ma)

Geochemical data indicate that the Oligocene to early Miocene interval (34–15 Ma) in the Eastern Paratethys was characterized by persistently low-oxygen conditions. The C_{org}/P ratio records suboxic to weakly anoxic values throughout this phase (Fig. 6a), defining a prolonged stratified interval known as the Maikop PBWS event. While the earlier Kuma Anoxic Event is marked by strong trace metal enrichments, the Maikop PBWS event shows only moderate Zn_{EF} and V_{EF} values and well pronounced Mo_{EF} peaks (Fig. 6b–d), suggesting a bottom-water oxygen depletion mechanism different from the Kuma Anoxia.

The early phase of the Maikop PBWS event is characterized by elevated C_{org}/P ratios, plotting within the high suboxic domain and peaking during the Chattian (Kalmykian), in parallel with strong enrichment in Mo_{EF} values. This interval reflects the culmination of bottom-water anoxia within the PBWS phase. Following this, both C_{org}/P and Mo_{EF} show signs of gradual decline, suggesting partial reoxygenation during the early Miocene (Fig. 6a, A6). A concurrent decrease in salinity from the mid-Chattian onwards—identified in the B/Ga and S/TOC records (Fig. 5, A2)—likely reflects regional hydrological change.

Our results also highlight two short-lived ventilation episodes interrupting the stratification regime, both clearly expressed in multiple geochemical proxies, including transient drops in C_{org}/P, rises in Sr/Ba, and decreases in S/TOC. These correspond to the Solenovian Event (c. 31.2 Ma) and a second event at c. 26.5–27 Ma (A4 and A5 in Figs. 5–6), with the latter also marked by increased B/Ga, suggesting temporary salinity recovery following a freshening pulse.

The onset and duration of the PBWS event are consistent with regional tectonic and oceanographic restructuring. The Oligocene marks the intensification of Alpine orogeny and a major global sea-level fall, both of which reduced the Eastern Paratethys's connectivity to open-marine systems (Popov et al., 1993, 2004; Schulz et al., 2005; van der Boon et al., 2019). Isotope data from SW Euxine basin (Tulan et al., 2020) indicates that the early stages of the Maikop PBWS event were characterized by $^{87}Sr/^{86}Sr$ values and trends similar to the Ocean water. Under these conditions, the basin developed estuarine-like circulation: saline marine inflow at depth and freshwater outflow at the surface inhibited vertical mixing and promoted stable stratification (Akhmetiev et al., 2012; Sachsenhofer et al., 2016; Baldi, 2006; Kováč et al., 2017; Boote et al., 2018; Sachsenhofer et al., 2018).

Our proxy data provide support for previously hypothesized transitions in Paratethys hydrology. The Solenovian and the 26.5 Ma events are not only expressed geochemically but also correlate closely with faunal turnover and lithological changes, including oolitic and marl-rich intervals interpreted as ventilation and transgression phases (İslamoğlu et al., 2008; Popov et al., 2022; Sachsenhofer et al., 2016). By the early Miocene, a decline in C_{org}/P and Mo_{EF} (Fig. 6a, A6), together with freshening trends in B/Ga and S/TOC (Fig. 5, A2), indicates partial reoxygenation and reduced salinity, aligning with regional uplift in the Greater Caucasus (Vincent et al., 2007) and increased runoff from the paleo-Laba River (Zaporozhets in Popov et al., 2019b). This hydrological reorganization coincides with the arrival of Mediterranean mollusk taxa (Popov et al., 2004), suggesting a new, albeit weaker, episode of connectivity during which a southerly marine corridor replaced the previously dominant North Atlantic connection.

The Maikop PBWS event interval represents a pivotal stage in the transformation of the Eastern Paratethys from an open-marine basin into a semi-isolated, intra-continental sea. This evolution was driven by a combination of tectonic uplift, eustatic sea-level changes, and regional hydrological reorganization. The persistence of suboxic conditions over several million years promoted biological isolation, leading to the emergence of endemic species adapted to unstable and stressed

environments (Soták, 2010), characterized by weak connections with the nearby oceanic basins.

Although intermittent connections to the North Atlantic facilitated occasional biotic exchange during the Oligocene (Popov et al., 2019b), these links diminished and ultimately ceased by the end of the period. Southern pathways—via former gateways to the Central Iranian and Mesopotamian basins—remained minimal and largely ineffective in sustaining marine exchange (Palcu et al., 2023). In the Early Miocene, however, new but weak marine connections began to develop, likely through extensional depressions associated with the Sivas Basin (Poisson et al., 2016). The Eastern Paratethys maintained more frequent and stable connectivity with the Central Paratethys, likely peaking during transgressive episodes throughout the Maikop PBWS phase. These intervals facilitated faunal exchange and the dispersal of endemic taxa between basins. Notable examples include the presence of shared Solenovian endemic faunal assemblages (Popov and Studencka, 2015) and the early Miocene migration of *Rzehakia dubiosa* from the Central Paratethys to the Eastern Paratethys (Popov et al., 2022).

6.3. Middle Miocene connectivity instability: changing seas in Paratethys

From the Middle Miocene to the Early Pliocene, the Eastern Paratethys was characterized by a series of paleoceanographic configurations that reflect changes in the connectivity with the global ocean. These changes were driven by regional tectonic activity, eustatic sea-level fluctuations, and climatic variations, which together influenced the exchange of water masses, salinity gradients, and biogeographic patterns. As a result, the Eastern Paratethys alternated between more isolated, restricted basinal conditions and phases of greater marine influence, leaving a complex sedimentary and faunal record that reflects its evolving hydrological and ecological state.

6.3.1. Return of open-marine connections in Central and Eastern Paratethys (Middle Miocene, 15.0–14.0 Ma)

Geochemical data from the Eastern Paratethys reveal a pronounced environmental shift between 15.0 and 14.0 Ma (Fig. 7), marked by the collapse of the Maikop PBWS event and the reintroduction of open-marine conditions. The B/Ga paleosalinity proxy shows a two-step increase: a modest rise from low-brackish values (B1), followed by a distinct marine influx at ~14.86 Ma (B2). The S/TOC proxy expresses a stronger and more sustained signal (B4), likely reflecting enhanced sensitivity to marine sulfate influx in carbonate-rich lithologies. After the influx, salinity stabilized at high-brackish values from ~14.8 to 14.4 Ma (B3), matching a phase of relative hydrological stability.

In parallel, the C_{org}/P proxy records the end of sustained suboxic conditions. Strongly suboxic values persisted just before the marine incursion (B5–B6) but were abruptly replaced by dominantly oxic conditions post-influx (B7), indicating the end of vertical stratification. A corresponding enrichment in trace metals (Mo, Zn, V) is recorded during this transition (B7), reflecting redox-sensitive element mobilization during reoxygenation.

This transition corresponds to the mid-Langhian (Badenian) transgression in the Central Paratethys, a major flooding event that reestablished connections with the Mediterranean and triggered widespread carbonate deposition (Kováč et al., 2007; Coric et al., 2009; Sant et al., 2017; Harzhauser et al., 2018). In the Eastern Paratethys, this interval aligns with the short-lived Tarkhanian stage, which followed the final phase of the Maikop Series. It is characterized by rising salinity, enhanced vertical water exchange, and improved oxygenation (Popov et al., 2023; Popov et al., 2019a). The Tarkhanian fauna, relatively diverse and dominated by brackish-marine species, support this interpretation and suggest salinity levels akin to the modern Black Sea (Görür et al., 2000; Palcu et al., 2017).

The sharp increase in salinity, collapse of stratification, and onset of oxic conditions indicated by B/Ga, S/TOC, and C_{org}/P proxies closely align with regional sedimentological and faunal indicators of renewed marine connectivity. Trace element enrichments provide additional evidence of a redox regime transition associated with this environmental shift.

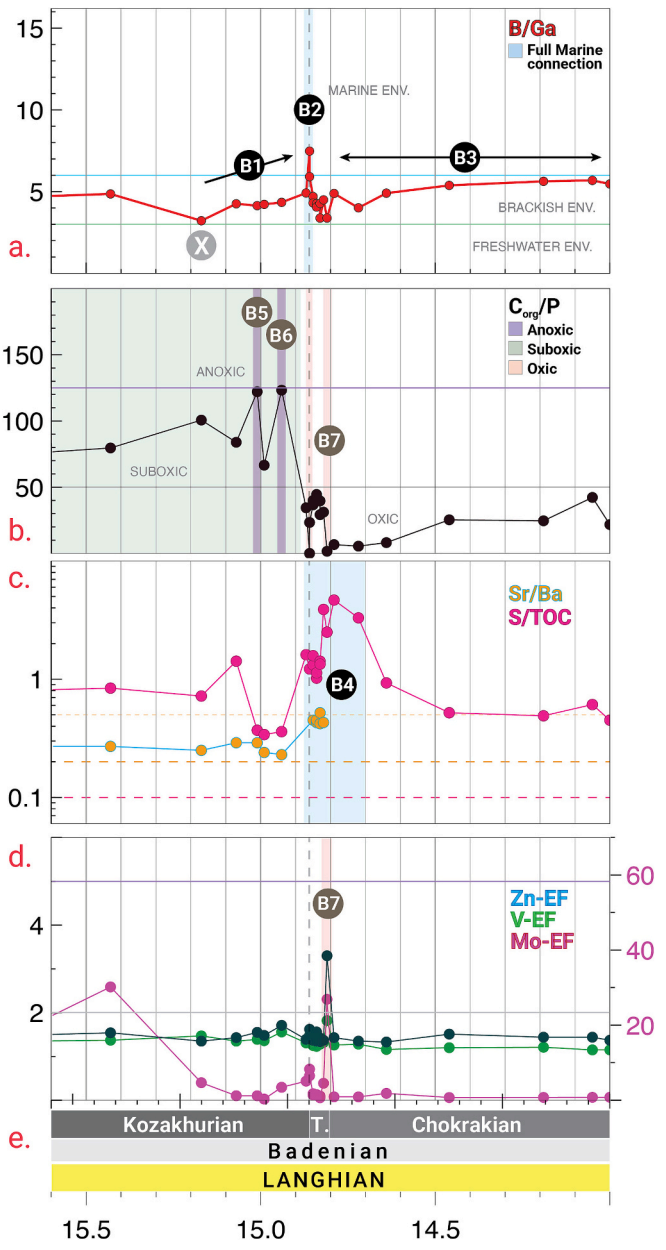

Fig. 7. The demise of the anoxic Paratethys Sea and its aftermath: (a) B/Ga showing a transition from low- to high-brackish salinities (B1), a marine influx at ~14.86 Ma (B2), and stabilization at high-brackish conditions (B3); **(b)** C_{org}/P indicates increasing stratification (B5–B6), collapse of anoxia at c. 14.86 Ma, and subsequent oxic stabilization (B7); **(c)** S/TOC also reflects this marine interval (B4), extending slightly beyond B3, likely due to carbonate influence; **(d)** Trace element enrichments correspond with the stable oxic regime onset (B7); **(e)** Timescale showing Eastern and Central Paratethys regional stages and global chronostratigraphy (Raffi et al., 2020).

The mid-Langhian (Badenian) transgression and its expression in the Eastern Paratethys during the Tarkhanian stage mark a pivotal point in Paratethyan paleoceanography. It terminated the Maikop PBWS event, reconnected the basin with open-marine circulation, and reestablished oxic bottom waters. This event laid the groundwork for subsequent environmental fluctuations by resetting basin stratification, redox state, and biogeochemical cycling.

6.3.2. Reverberations of connectivity change: Karaganian restriction and unification during the BSEE/KVT events (Middle Miocene, 14.0–12.4 Ma)

Following the marine peak at ~14.86 Ma, geochemical proxies document a return to restricted conditions across the Eastern Paratethys.

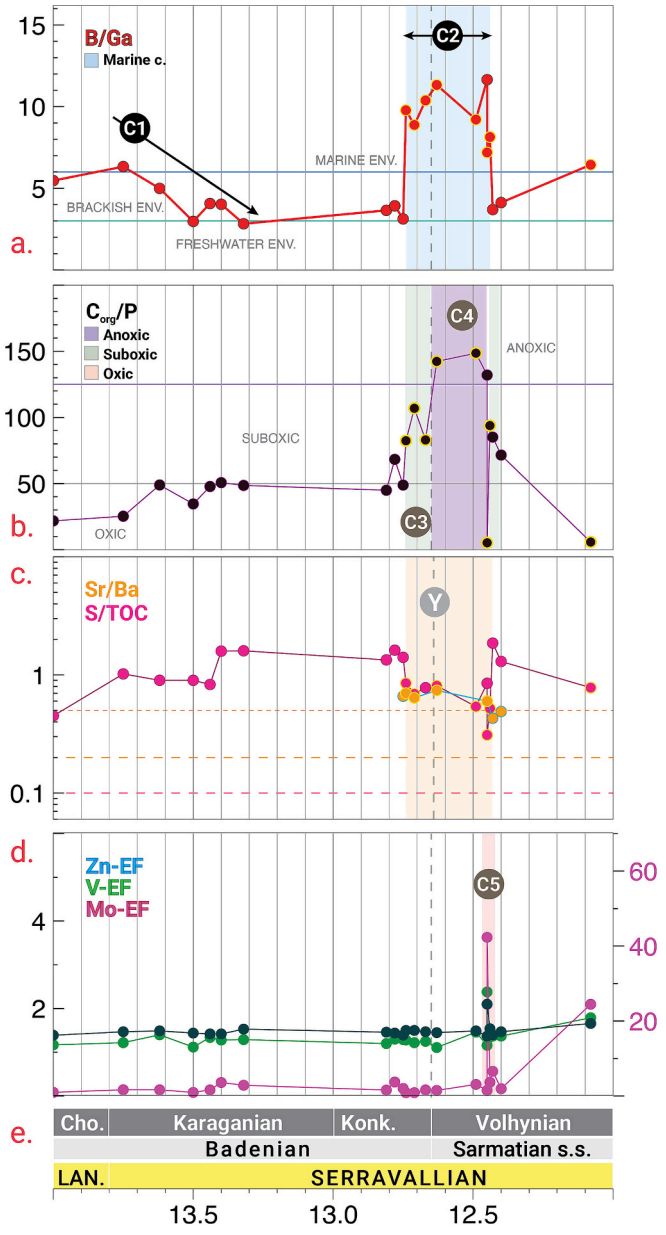

Fig. 8. The Konkian–Volhynian boundary (Y) and the Eastern Paratethys response to the Badenian–Sarmatian Extinction Event (BSEE): (a) B/Ga indicates a gradual salinity decrease from normal marine to low-brackish values (C1) between c. 14 and 13.3 Ma, followed by a short-lived increase to marine values between c. 12.8 and 12.4 Ma (C2), coinciding with the BSEE at 12.65 Ma; **(b)** C_{org}/P shows a shift from oxic to suboxic conditions during the marine interval (C3), culminating in anoxic values (C4), with oxygenation recovery following the marine pulse; **(c)** S/TOC shows a drop in values that nevertheless plot as marine while Sr/Ba show marine values followed by a decrease to brackish (C5); **(d)** Trace element enrichments (C5) occur during after the end of the brief anoxic episode highlighting redox instability linked to connectivity changes; **(e)** Timescale showing Eastern Paratethys regional stages, Central Paratethys regional stages, and global chronostratigraphy (Raffi et al., 2020). Data points from the Panagia section are highlighted with yellow contours in panels (a–c); all other points represent samples from the Belaya section. (For interpretation of the references to colour in this figure legend, the reader is referred to the web version of this article.)

The B/Ga record shows a gradual decline in salinity from ~14.0 to ~13.5 Ma (Fig. 8, C1), with low-brackish conditions persisting until ~12.8 Ma. This period is marked by stratified water columns and faunal impoverishment, with shallow, oxygen-stressed habitats dominated by Barnea spp.

Between 12.8 and 12.4 Ma, a short-lived marine pulse is observed, with B/Ga values temporarily rising (C2). This coincides with the Badenian–Sarmatian Extinction Event (BSEE) in the Central Paratethys and the Konkian–Volhynian Transition (KVT) in the Eastern Paratethys. Despite the marine nature of this pulse, it corresponds with a sharp faunal decline. The C_{org}/P proxy records a drop in oxygenation from oxic to suboxic (C3), culminating in full anoxia by ~12.65 Ma (C4). Trace element enrichments (C5) follow this anoxic phase, suggesting a short reoxygenation episode and strong redox gradients.

The BSEE, dated to ~12.65 Ma (Palcu et al., 2015), represents a major faunal turnover triggered by shifting marine gateways and internal mixing between the saltier Central and low-brackish Eastern Paratethys (Harzhauser and Piller, 2007; Palcu et al., 2017). In the Eastern Paratethys, this is expressed as the KVT, associated with extinction of endemic mollusks and foraminifera, followed by simplified, opportunistic faunal assemblages (Nevesskaya et al., 2005; Nevesskaya et al., 1986). While the Central Paratethys experienced salinity decline (Studencka and Jasionowski, 2011), the Eastern Paratethys basin briefly saw salinity rise, followed by a strong desalination trend during the Bessarabian and Khersonian stages.

The marine pulse captured in B/Ga (C2), the redox shift in Corg/P (C3–C4), and the trace metal enrichment during the reoxygenation phase (C5) all align with the proposed timing and impact of the BSEE/KVT events. These geochemical records validate the hypothesis of transient marine influx, subsequent stratification, and biotic stress driven by fluctuating basin connectivity.

The BSEE/KVT events reflect a critical feedback phase in Paratethyan evolution, where interbasinal mixing after marine reconnection led to ecosystem collapse rather than recovery. These events underscore the fragility of semi-enclosed basins to salinity-driven thresholds and highlight how rapid shifts in connectivity can cause cascading biogeochemical and ecological consequences. This interval marks a transition toward a more isolated, less resilient Eastern Paratethys system that would persist through the Late Miocene.

6.4. Late Miocene isolation and reconnections with the Mediterranean

6.4.1. Megalake Paratethys – a landlocked aquatic system (11.6–6.7 Ma)

Geochemical records from the Eastern Paratethys during the Late Miocene capture the transition to a landlocked megalake regime. The B/Ga paleosalinity proxy indicates generally stable salinity conditions in the high-brackish to marine range from ~11.6 to 7.6 Ma (Fig. 9, D1), punctuated by discrete episodes of salinity reduction alternating with episodes of increase. These declines and increases likely reflect internal lake-level variability and hydrological compartmentalization.

The C_{org}/P redox proxy shows that the basin remained predominantly suboxic throughout this interval, with three distinct anoxic episodes recorded at ~9.7 Ma, ~9.4 Ma, and ~ 7.6 Ma (Fig. 9, D2–D4). These phases are interspersed with brief oxic excursions, particularly one at ~7.6 Ma (D5–D6), also marked by increases in Mo, Zn, and V enrichment (D6), suggesting transient redox reorganization and trace metal mobilization. The persistence of suboxic conditions alongside limited salinity fluctuations reflects a central basin setting buffered against short-term hydrological instability.

Importantly, **our paleosalinity proxies—including B/Ga, Sr/Ba, and S/TOC—do not record a strong or sustained signal of marine transgression during the Maeotian transgressive interval at 7.6 Ma** (Fig. 9, Z). Instead, **B/Ga values remain within the same range as those observed during prior megalake fluctuations**, indicating that **any increase in salinity was relatively modest and transient**. This absence of a clear transgressive signal suggests that the observed

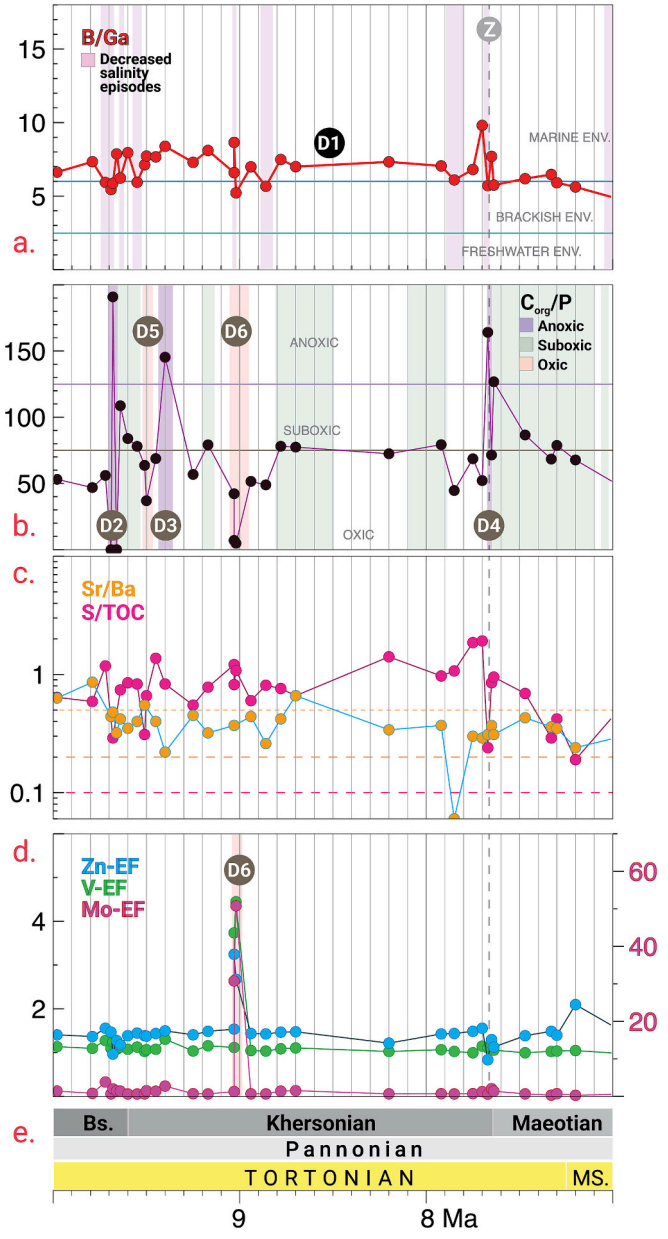

Fig. 9. Evolution of Megalake Paratethys during the Late Miocene: (a) B/Ga indicates stable marine to brackish-marine salinities, with brief salinity decreases (D1), a short-lived increase just prior to the Maeotian Flooding Event (Z), and subsequent stabilization at high-brackish levels; **(b)** C_{org}/P shows a dominantly suboxic regime with highly fluctuating values, interrupted by three anoxic episodes at 9.7 Ma, 9.4 Ma, and 7.6 Ma (D2–D4), and two oxic excursions (D5 and D6); **(c)** S/TOC and Sr/Ba support this redox evolution, with values aligning with major salinity and ventilation shifts; **(d)** Trace element enrichments occur during the oxic excursion at 7.6 Ma (D6), highlighting redox sensitivity to basin reoxygenation events; **(e)** Timescale showing the Eastern Paratethys regional stages, Central Paratethys regional stages, and global chronostratigraphy (Raffi et al., 2020).

changes were likely due to internal hydrological reorganization or interbasinal mixing, rather than a true reconnection with the global ocean.

The merging of the Central and Eastern Paratethys into a single, vast inland waterbody—referred to as the Megalake Paratethys—occurred in the aftermath of the BSEE and was driven by progressive tectonic closure of oceanic connections, notably the Slovenian Corridor (Bartol et al., 2014; Palcu et al., 2021). After initial expansion, regional base-level changes led to episodic fragmentation and reconnection within the megalake system, with highstand phases promoting stratification and lowstand phases causing freshwater desalination in perched sub-basins (Popov et al., 2010; Butiseacă et al., 2021; Goldin et al., 2020).

The onset of this forced regressive hydrological regime is dated to ~9.9 Ma in the Caspian Basin (Lazarev et al., 2025) and ~ 9.7 Ma in the Kuban Basin (Palcu et al., 2021), culminating in a regional transgression at ~7.6 Ma that marks the beginning of the Maeotian (Lazarev et al., 2020; Palcu et al., 2019b). This event coincided with a brief rise in salinity and interbasinal exchange (Popov et al., 2016). However, some studies have interpreted this as a more substantial marine incursion (REFS).

During the late Maeotian and into the Pontian, faunal records show increased dominance of euryhaline taxa such as *Congeria* and *Theodoxus*, as well as the appearance of freshwater ostracods (Stoica et al., 2016; Popov et al., 2022). Marine incursions during this time occasionally introduced diatoms and nannoplankton, indicating episodic but non-persistent marine influence (Radionova et al., 2012).

While earlier interpretations have proposed that the Maeotian transgression was a significant marine event, **our geochemical evidence contradicts this view**. The B/Ga and complementary paleosalinity proxies indicate only limited salinity increase during the Maeotian and do not support a robust marine inflow. This matches a growing body of regional evidence that reinterprets the Maeotian transgression as a **localized or intra-Paratethyan phenomenon**, rather than a re-establishment of global oceanic connections. The faunal turnover and transient increases in marine biota may instead reflect interbasinal mixing or basin internal dynamics.

The Megalake Paratethys represents one of the most dynamic landlocked aquatic systems of the Neogene. This interval demonstrates how large, internally drained basins can retain relatively stable chemical signatures even while experiencing significant ecological and hydrological oscillations. The absence of a strong marine signature during the Maeotian transgression emphasizes the role of internal base-level and basin-wide connectivity shifts in shaping salinity, oxygenation, and trace element cycling. These findings refine our understanding of the timing and magnitude of Paratethyan isolation and underscore the importance of multi-proxy approaches in distinguishing between true oceanic influence and internal reorganization in marginal marine systems.

6.4.2. Late Miocene-early Pliocene reconnections with the Mediterranean (6.7–4.4 Ma)

Our geochemical records capture the final phase of the Paratethys megalake and the progressive hydrological re-engagement with the Mediterranean realm. The B/Ga proxy reveals a brief return to higher salinity values between 6.7 and 6.5 Ma (Fig. 10, E1), consistent with a short-lived marine influx following the Intra-Maeotian Event (IME). This is followed by a prolonged interval of brackish conditions from 6.5 to 5.6 Ma, with **no discernible paleosalinity signal corresponding to the well-documented Pontian transgression at 6.1 Ma** (Fig. 10, V). These stable B/Ga values suggest the absence of substantial salinity change, likely reflecting the basin's buffered geochemical regime.

During the latest Miocene regional Pontian stage, B/Ga ratios decline further, approaching low-brackish thresholds (Fig. 10, E2), suggesting that the Eastern Paratethys functioned as a dilution basin at that time, possibly due to increased freshwater input and isolation-driven desalination. The complementary salinity proxies Sr/Ba and S/TOC support this interpretation, recording similar trends toward reduced salinity.

The C_{org}/P redox proxy shows suboxic conditions during the IME, including a brief episode of anoxia, likely coinciding with the marine influx at ~6.7 Ma (Fig. 10, E3). In contrast, the Pontian interval is marked by predominantly oxic conditions with isolated suboxic values. Crucially, **trace element enrichments (Mo_{EF}, Zn_{EF}, V_{EF}) are absent throughout this interval**, indicating that **bottom-water anoxia was weak or transient** and that the basin remained relatively well

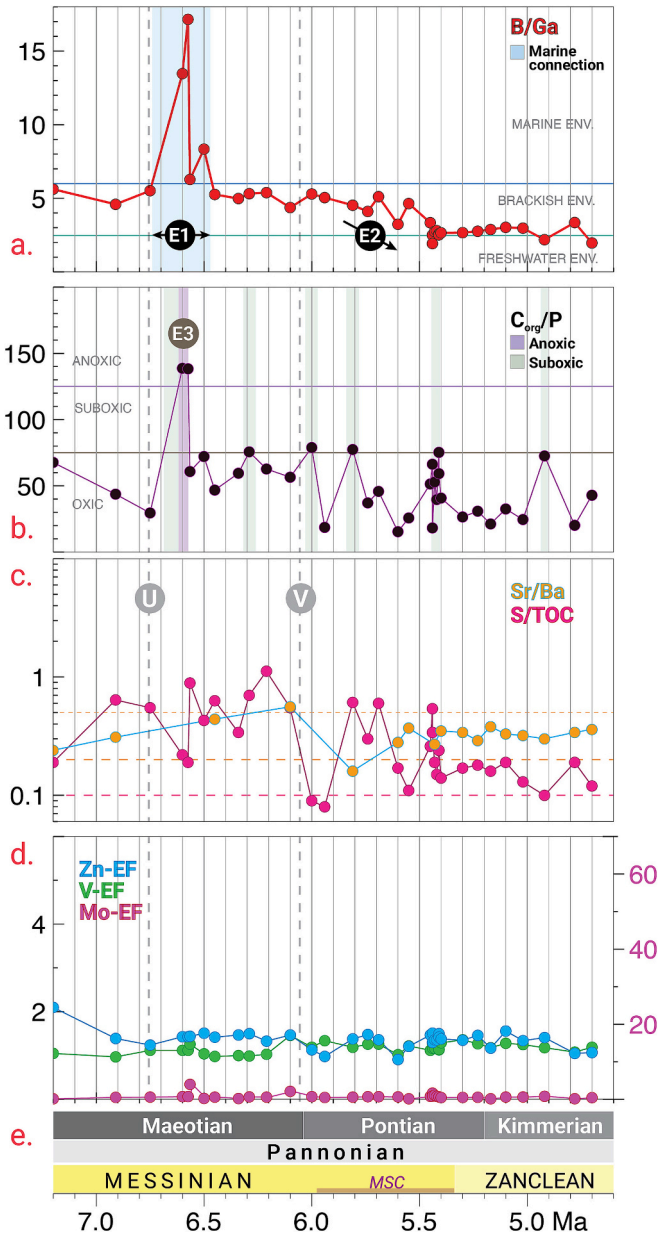

Fig. 10. Reconnection of Megalake Paratethys with the Mediterranean Sea: (a) B/Ga indicates a brief marine interval (E1) between c. 6.7 and 6.4 Ma coinciding with the aftermath of the Intra-Maeotian Event (U). This is followed by a declining salinity phase (E2) between c. 6.3 and 5.5 Ma, followed by a stable interval with values close to freshwater until c. 4.4 Ma; **(b)** C_{org}/P data show a complex picture dominated by (sub)oxic values (7.2–5.0 Ma), with a brief interval at 6.6 Ma characterized by anoxic values (E3) coinciding with the marine interval (A). The younger part is dominated by oxic signature with occasional suboxic values; **(c)** Sr/Ba and S/TOC; **(d)** Trace element enrichments are missing from this interval; **(e)** Timescale showing the Eastern Paratethys regional stages, Central Paratethys regional stages and Global Stratigraphic units (Raffi et al., 2020).

ventilated, even during periods of base-level drop.

The Paratethys megalake phase represents a period of prolonged disconnection from the global ocean, bounded by the closure of the Middle Miocene marine gateways via Central Europe and the eventual onset of marine reconnection with the Mediterranean via the Aegean realm (Krijgsman et al., 2020a, 2020b). The broader Mediterranean region experienced its own disconnection from the Atlantic during this time, culminating in the Messinian Salinity Crisis (MSC), dated between 5.97 and 5.33 Ma (Roveri et al., 2014; Krijgsman et al., 2024), and characterized by partial desiccation and widespread evaporite deposition.

In the Eastern Paratethys, the first recognized indication of renewed communication with the Mediterranean occurs in the wake of the IME (~6.8–6.7 Ma; Palcu et al., 2019b), which has been interpreted as a eustatic-driven intra-Paratethyan event (Golovina et al., 2019; Radionova and Golovina, 2010). Some earlier hypotheses proposed dramatic base-level drops during the MSC (up to 1 km; Hsü and Giovanoli, 1979), particularly in the Black Sea Basin (Gillet et al., 2007; Munteanu et al., 2012). However, more recent work has favored conservative scenarios involving base-level decreases of ~100 m (Krijgsman et al., 2010; van Baak et al., 2016, 2017), with a drawdown at ~5.6 Ma (Rostovtseva and Rybkina, 2017).

Our results refine and partly revise the existing narrative. While the IME is recorded as a minor marine event in both literature and our data, **the expected salinity signal associated with the Pontian transgression at ~ 6.1 Ma is notably absent**. Likewise, our proxies show **no support for extreme MSC-related desiccation in the Eastern Paratethys**, instead pointing to a basin that remained brackish and relatively oxygenated during this time and later, toward the final stage of the MSC switching to a low–brackish environments, a salinity decrease that although not precisely constrained chronologically points to desalination of Paratethys, probably due to increase outflow toward the partially desiccated Mediterranean. The C_{org}/P and trace element proxies confirm the lack of persistent stratification or deep-water anoxia, which is consistent with newer interpretations favoring mild base-level decline and limited isolation.

This interval marks the end of the Paratethys as a fully isolated system and its slow transition toward re-integration with the Mediterranean and global ocean circulation. The brief marine episodes recorded after the IME and the subdued salinity signal during the MSC suggest that the Eastern Paratethys remained largely decoupled from dramatic Mediterranean desiccation events. These findings support the emerging paradigm that **the Eastern Paratethys operated as a semi-isolated, buffered system** during the latest Miocene, with limited sensitivity to global eustatic extremes.

7. Paleoenvironmental evolution of the aquatic systems of central Eurasia (42–4 Ma)

The Tethys and Paratethys realms in Eurasia provide an exceptional geological archive encompassing nearly 40 million years of Earth's history, allowing for a comprehensive examination of the paleoenvironmental evolution of aquatic systems during pivotal geological intervals. This extensive record facilitates the observation of diverse environmental iterations that have been intricately shaped by fluctuations in ocean connectivity, thereby delineating significant archetypes of paleoenvironmental change.

The geological record of the Tethys-Paratethys realm documents two distinct modes of water stratification and anoxia, particularly during the Kuma (42–34 Ma; Sachsenhofer et al., 2018) and Maikop (34–15 Ma; van der Boon et al., 2019; Palcu et al., 2019a) intervals. The Kuma Anoxic Event is postulated to have developed under conditions akin to localized oceanic anoxic events, characterized by substantial influxes of trace elements and the deposition of organic-rich sediments. Geochemical profiles from this period reveal elevated C_{org}/P ratios, indicating significant stratification and restricted oxygenation. Conversely, the Maikop PBWS event is representative of a eutrophic scenario typical of a closed epicontinental sea, wherein reduced marine connectivity resulted in stagnant water columns and elevated organic productivity. The organic-rich sediments associated with the Maikop Series serve as a critical record of these conditions, encapsulating the ecological ramifications of prolonged anoxia and stratification within the basin. A comparative analysis of the geochemical signatures stemming from these two intervals of anoxia—the Kuma anoxic event and

Maikop PBWS event—may yield valuable insights and methodological advancements for disentangling complex geological signals documented in the sedimentary record. By elucidating the environmental contexts governing each episode, this research contributes to a broader understanding of how analogous anoxic conditions may have been manifested in other sedimentary basins worldwide, enhancing our capacity to interpret ancient marine systems and their responses to past global changes.

Throughout this extended temporal framework, two principal modes of paleoenvironmental change are evident: (1) long-term trends and (2) short-lived perturbations linked to tectonic and oceanographic events that modulated marine connectivity (Popov et al., 2004; Rögl, 1999; Harzhauser and Piller, 2007). A major long-term trend is the gradual decline in salinity during the early Miocene, corresponding to the Maikopian anoxic interval (~23–15 Ma). This sustained freshening trend marks a critical phase of hydrological and ecological transformation, driven by increased restriction from global marine waters (van der Boon et al., 2019; Palcu et al., 2019a; Popov et al., 2023). The trend reflects progressive basin isolation, a feature typical of the Eastern Paratethys due to narrowing gateways and evolving basin morphology (Popov et al., 2004; Krijgsman et al., 2020a, 2020b). In contrast, abrupt salinity excursions correspond with transient marine incursions that briefly enhanced connectivity. Key examples include the **mid-Langhian marine transgression** (~14.8 Ma), associated with the **Badenian–Tarkhanian flooding** (Palcu et al., 2019a; Sant et al., 2019a,b; Harzhauser and Piller, 2007); the **Badenian–Sarmatian Extinction Event (**Harzhauser and Piller, 2007; Liu et al., 2017; Palcu et al., 2015**) and** the **Konkian–Volhynian transition (**Palcu et al., 2017; Lazarev et al., 2025**),** which reflect mixing between the Central and Eastern Paratethys watermasses (Palcu et al., 2017, Popov et al., 2022); and the **marine incursions following the Intra-Maeotian Event** (~6.7 Ma), which left a discernible imprint on regional salinity and biotic (Golovina et al., 2019, Golovina and Radionova, 2010).

Additionally, the transition toward outflow-only configurations during the latest Miocene to earliest Pliocene mirrors patterns observed during partial desiccation phases of the Paratethys megalake in the Tortonian (Palcu et al., 2021). In such scenarios, partial desiccation of a landlocked lacustrine system typically results in desalination of marginal basins, while salinity increases in more central, isolated depocenters. When applied to the **Messinian Salinity Crisis** (5.97–5.33 Ma) paleogeographic context (Krijgsman et al., 2024; Garcia-Castellanos and Villaseñor, 2011; Roveri et al., 2014), this framework suggests a partially desiccated Mediterranean fragmented into low-lying, hypersaline sub-basins, fed by a perched Paratethys system experiencing parallel desalination processes.

8. Methodological considerations and proxy limitations

Our results demonstrate that the B/Ga ratio emerges as the most robust and reliable proxy for reconstructing paleosalinity in the Paratethys. It shows strong consistency with paleontological data, outperforming complementary geochemical indicators such as Sr/Ba and S/TOC. While Sr/Ba and S/TOC can offer limited supporting insights, their applicability is notably reduced in the context of the Paratethys. These proxies often yield more ambiguous or indirect signals, making B/Ga the preferred and most diagnostic tool for paleosalinity reconstructions (Liu et al., 2025; Liu et al., 2024; Wei and Algeo, 2020). However, our results indicate boron in sediments remains a notable limitation, necessitating careful cross-validation with independent paleontological, geochemical and sedimentological data to ensure reliability.

Similarly, the C_{org}/P proxy proves to be more reliable for interpreting Paratethys paleoventilation conditions than trace element enrichment data when cross-validated with paleontological, geochemical and sedimentological data from the other studies. Trace element enrichments, while informative, appear to be more closely linked to the collapse of anoxia and the subsequent stabilization of geochemical conditions within the basin. This relationship highlights the episodic nature of trace element enrichment, which often coincides with shifts from anoxic to oxic conditions. For instance, enrichments in zinc, vanadium and molybdenum are typically associated with post-anoxic intervals characterized by geochemical stability rather than the direct presence of anoxia itself.

At this stage, however, our data cannot fully resolve the superposition of local and regional signals within each stratigraphic interval. Riverine input, coastal morphology, and sedimentary conditions can significantly influence geochemical proxies—especially in shallow or marginal marine settings. Yet, despite the lithological and geographic differences between the Belaya and Panagia sections, both show consistent geochemical transitions across the Konkian–Volhynian boundary. This internal agreement, visualized in Fig. 8, suggests that broad regional signals are preserved and can be extracted, particularly when multiple independent sections are compared.

This convergence emphasizes a broader methodological insight: to effectively disentangle local variability from regional environmental trends, it is necessary to expand the number of high-resolution, parallel records using standardized analytical approaches. Notably, intervals of geochemical stability—characterized by gradual trends rather than abrupt perturbations—are more suitable for inter-regional comparisons. In contrast, transitional phases may suffer from diachrony, resolution mismatch, and local overprinting, making them more difficult to correlate meaningfully across basins.

Consequently, we caution that the results of this study should not be taken at face value in a strictly quantitative sense. While the patterns identified here represent significant advances in understanding Paratethyan paleoenvironmental evolution, they also reflect the early stages of geochemical exploration in this complex, semi-isolated system. Given the pronounced interplay between local and regional factors—including tectonics, basin morphology, fluvial input, and diagenesis—proxy values must be interpreted with a degree of caution and within their broader stratigraphic and sedimentological contexts.

In this framework, the most valuable insights lie in the observed trends, phase relationships, and qualitative shifts rather than absolute values. These broader signals provide the clearest window into long-term environmental changes. Establishing these baseline trends and identifying recurring geochemical patterns for a range of stratigraphically and geographically diverse settings is the first essential step toward a fully resolved, integrated model of Paratethys evolution.

Moving forward, further integration of geochemical, stratigraphic, and biotic datasets across a larger spatial and temporal framework will be key to refining the precision and interpretive power of these proxies. Until then, studies such as this must serve as foundational references—prioritizing reproducibility and qualitative coherence over quantitative interpretations—and guiding future high-resolution work aimed at unraveling the complex history of the Paratethys realm.

9. Conclusions

The Paratethys realm serves as a remarkable example of the interplay between tectonic, climatic and oceanographic processes that shaped its paleoenvironmental evolution from the Middle Eocene to the Pliocene. Our study highlights the transformative role of marine connectivity, salinity fluctuations and redox conditions in driving its dynamic history. By applying robust elemental proxies such as B/Ga, Sr/Ba and S/TOC ratios, alongside paleoventilation indicators like C_{org}/P and trace metal enrichment factors, we have developed a comprehensive framework to reconstruct the basin's hydrological and geochemical history.

The findings elucidate key transitions in the basin, such as the progressive isolation during the Oligocene, the dominance of anoxia during the Kuma and persistent basin water stratification during Maikop intervals and the hydrological instability of the Late Miocene Megalake Paratethys system. The B/Ga proxy proved to be the most reliable indicator of paleosalinity, effectively capturing marine influxes, while Sr/

Ba and S/TOC provided complementary insights into specific hydrological changes. Similarly, the C_{org}/P ratio emerged as the primary tool for understanding paleoventilation, surpassing the reliability of trace element enrichments, which are more closely tied to post-anoxic stabilization phases.

Future research should aim to refine the chronology of these transitions and expand the spatial coverage of proxy-based studies to capture the full complexity of the Paratethys' environmental dynamics. By doing so, the Paratethys can continue to serve as a vital archive for understanding the interconnections between paleogeography, geochemistry and global climate during the Cenozoic.

CRediT authorship contribution statement

Dan V. Palcu Rolier: Writing – review & editing, Writing – original draft, Visualization, Validation, Supervision, Resources, Project administration, Methodology, Investigation, Funding acquisition, Formal analysis, Conceptualization. **Zhanhong Liu:** Writing – original draft, Methodology, Investigation, Formal analysis, Conceptualization. **Wei Wei:** Writing – original draft, Supervision, Methodology, Investigation, Formal analysis, Conceptualization. **Sergey Popov:** Writing – review & editing, Writing – original draft, Validation, Methodology, Investigation. **Larisa Golovina:** Writing – original draft, Validation, Investigation. **Iuliana Vasiliev:** Writing – original draft, Validation, Investigation. **Wout Krijgsman:** Writing – original draft, Visualization, Validation, Supervision, Investigation, Conceptualization. **Thomas Algeo:** Writing – review & editing, Writing – original draft, Validation, Supervision, Methodology, Investigation, Formal analysis, Data curation, Conceptualization.

Declaration of competing interest

The authors declare that they have no known competing financial interests or personal relationships that could have appeared to influence the work reported in this paper.

Acknowledgments

Funding: This publication is part of the project "Impact of sea-level rise on anoxic basins: Paratethys vs. Black Sea" [grant Veni.212.136] of the research Talent programmed – Veni which is financed by the Dutch Research Council (NWO) of DVP. DVP also acknowledges Project PNRR C9 – I8 "Multiproxy reconstruction of Eurasian Megalakes, connectivity and isolation patterns during Neogene-Quaternary times", code 97/15.11.2022, Contract No. 760115/23.05.2023.

Appendix A. Supplementary data

Supplementary data to this article can be found online at https://doi.org/10.1016/j.chemgeo.2025.122974.

Data availability

No data was used for the research described in the article.

References

Akhmetiev, M.A., Popov, S.V., Krhovsky, J., Goncharova, I.A.A., Zaporozhets, N.I.I., Radionova, E.P.P., 1995. Paleontology and stratigraphy of the Eocene-Miocene sections of the western Pre-Caucasia.

Akhmetiev, M.A., Zaporozhets, N.I., Benyamovskiy, V.N., Aleksandrova, G.N., Iakovleva, A.I., Oreshkina, T.V., 2012. The paleogene history of the western Siberian seaway - a connection of the Peri-Tethys to the Arctic Ocean. Austrian J. Earth Sci. 105, 50–67.

Algeo, T.J., Ingall, E., 2007. Sedimentary C_{org}:P ratios, paleocean ventilation and Phanerozoic atmospheric pO_2. Palaeogeogr. Palaeoclimatol. Palaeoecol. 256 (3–4), 130–155.

Algeo, T.J., Li, C., 2020. Redox classification and calibration of redox thresholds in sedimentary systems. Geochim. Cosmochim. Acta 287, 8–26.

Algeo, T.J., Tribovillard, N., 2009. Environmental analysis of paleoceanographic systems based on molybdenum–uranium covariation. Chem. Geol. 268 (3–4), 211–225.

Algeo, T.J., Wei, W., Sweet, D.E., 2025. Salinity variation in Carboniferous cyclothemic successions. Chem. Geol. 683, 122760.

Allen, M.B., Armstrong, H.A., 2008. Arabia–Eurasia collision and the forcing of mid-Cenozoic global cooling. Palaeogeogr. Palaeoclimatol. Palaeoecol. 265, 52–58. https://doi.org/10.1016/j.palaeo.2008.04.021.

Baldi, K., 2006. Paleoceanography and climate of the Badenian (Middle Miocene, 16.4–13.0 Ma) in the Central Paratethys based on foraminifera and stable isotope (δ18O and δ13C) evidence. International Journal of Earth Sciences 95 (1), 119–142.

Bartol, M., Mikuž, V., Horvat, A., 2014. Palaeontological evidence of communication between the Central Paratethys and the Mediterranean in the late Badenian/early Serravalian. Palaeogeogr. Palaeoclimatol. Palaeoecol. 394, 144–157. https://doi.org/10.1016/j.palaeo.2013.12.009.

Beniamovski, V., Alekseev, A., Ovechkina, M.N., Oberhansli, H., 2003. Middle to Upper Eocene dysoxic-anoxic Kuma Formation (northeast Peri-Tethys): Biostratigraphy and paleoenvironments. In: Wing, S.L., Gingerich, P.D., Schmitz, B., Thomas, E. (Eds.), Causes Consequences Glob. Warm Clim, Early Paleogene, Geol Soc Am, Boulder, Colorado, pp. 95–112.

Berner, R.A., 1980. Early Diagenesis: A Theoretical Approach. Princeton University Press, Princeton.

Bohaty, S.M., Zachos, J.C., 2003. Significant Southern Ocean warming event in the late middle Eocene. Geology 31, 1017–1020. https://doi.org/10.1130/G19800.1.

Boote, D.R.D.D., Sachsenhofer, R.F., Tari, G., Arbouille, D., 2018. Petroleum provinces of the Paratethyan region. J. Pet. Geol. 41, 247–297. https://doi.org/10.1111/jpg.12703.

Butiseacă, G.A., Vasiliev, I., van der Meer, M.T.J., Krijgsman, W., Palcu, D.V., Feurdean, A., Niedermeyer, E.M., Mulch, A., 2021. Severe late Miocene droughts affected western Eurasia. Glob. Planet. Chang. 206. https://doi.org/10.1016/j.gloplacha.2021.103644.

Coric, S., Pavelic, D., Rögl, F., Mandic, O., Vrabac, S., Avanic, R., 2009. Revised middle Miocene datum for initial marine flooding of North Croatian basins (Pannonian basin system, central Paratethys). Geol Croat 62, 31.

Cramwinckel, M.J., van der Ploeg, R., van Helmond, N.A.G.M., Waarlo, N., Agnini, C., Bijl, P.K., 2023. Deoxygenation and organic carbon sequestration in the Tethyan realm associated with the middle Eocene climatic optimum. Geol. Soc. Am. Bull. 135, 1280–1296. https://doi.org/10.1130/B36280.1.

Darin, M.H., Umhoefer, P.J., Thomson, S.N., 2018. Rapid late Eocene Exhumation of the Sivas Basin (Central Anatolia) Driven by initial Arabia-Eurasia Collision. Tectonics 37, 3805–3833. https://doi.org/10.1029/2017TC004954.

Filippova, N.Y., Beluzhenko, E.V., Golovina, L.A., 2015. On the Paleogene-Neogene boundary and age of the Alkun Formation in the North Caucasus and Ciscaucasia. Stratigr. Geol. Correl. 23, 620–644. https://doi.org/10.1134/s0869593815060052.

Garcia-Castellanos, D., Villaseñor, A., 2011. Messinian salinity crisis regulated by competing tectonics and erosion at the Gibraltar arc. Nat. Geosci. 4, 469–473. https://doi.org/10.1038/ngeo1205.

Gavrilov, Y.O., Kopaevich, L.F., 1996. Some of the geochemical, biochemical and biotic consequences of eustatic oscillations. Stratigr. Geol. Correl. 4, 315–325.

Gavrilov, Y.O., Shcherbinina, E.A., Muzylöv, N.G., 2000. A Paleogene sequence in central North Caucasus: a response to paleoenvironmental changes. GFF 122, 51–53. https://doi.org/10.1080/11035890001221051.

Gavrilov, Y.O., Shchepetova, E.V., Shcherbinina, E.A., Golovanova, O.V., Nedumov, R.I., Pokrovsky, B.G., 2017. Sedimentary environments and geochemistry of Upper Eocene and lower Oligocene rocks in the northeastern Caucasus. Lithol. Miner. Resour. 52, 447–466. https://doi.org/10.1134/S0024490217060037.

Gavrilov, Y., Nedumov, R., Shchepetova, E., Shcherbinina, E., Kozlova, E., Golovanova, O., 2021. Stratigraphy, sedimentology and geochemistry of the Oligocene – lower Miocene Maikop Group in Dagestan, NE Caucasus. J. Pet. Geol. 44, 385–412. https://doi.org/10.1111/jpg.12798.

Gillet, H., Lericolais, G., Réhault, J.P., 2007. Messinian event in the Black Sea: evidence of a Messinian erosional surface. Mar. Geol. 244, 142–165. https://doi.org/10.1016/j.margeo.2007.06.004.

Goldin, P., Haiduc, B.S., Kovalchuk, O., Górka, M., Otryazhyi, P., Brânzilă, M., 2020. The Volhynian (late Middle Miocene) marine fishes and mammals as proxies for the onset of the Eastern Paratethys re-colonisation by vertebrate fauna. Palaeontol. Electron. 23, 1–20. https://doi.org/10.26879/1091.

Golovina, L.A., Radionova, E.P., van Baak, C.G.C., Krijgsman, W., Palcu, D.V., 2019. A late Maeotian age (6.7–6.3 Ma) for the enigmatic "Pebbly Breccia" unit in DSDP Hole 380A of the Black Sea. Palaeogeogr. Palaeoclimatol. Palaeoecol. 533, 109269. https://doi.org/10.1016/j.palaeo.2019.109269.

Golovina, L.A., Bylinskaya, M.E., Popov, S.V., Golovina, E.D., 2024. New data on the nannofossil and planktonic foraminiferal composition in the lower Miocene Alkun Formation, Ciscaucasia. Stratigr. Geol. Correl. 32, 420–433. https://doi.org/10.1134/S0869593824700084.

Görür, N., Çağatay, N., Sakinç, M., Akkök, R., Tchapalyga, A., Natalin, B., 2000. Neogene Paratethyan succession in Turkey and its implications for the palaeogeography of the Eastern Paratethys. Geol. Soc. Spec. Publ. 173, 251–269. https://doi.org/10.1144/GSL.SP.2000.173.01.13.

Grossheim, V.A., 1960. The Paleogene of the northwestern Caucasus. Tr Krasn Fil VNIGRI Moscow Gostoptekhizdat 4, 190.

Habicht, K.S., Canfield, D.E., 1997. Sulfur isotope fractionation during bacterial sulfate reduction in organic-rich sediments. Geochim. Cosmochim. Acta 61 (24), 5351–5361. https://doi.org/10.1016/S0016-7037(97)00311-6.

Harzhauser, M., Piller, W.E., 2007. Benchmark data of a changing sea – Palaeogeography, palaeobiogeography and events in the Central Paratethys during the Miocene. Palaeogeogr. Palaeoclimatol. Palaeoecol. 253, 8–31. https://doi.org/10.1016/j.palaeo.2007.03.031.

Harzhauser, M., Grunert, P., Mandic, O., Lukeneder, P., Gallardo, Á.G., Neubauer, T.A., 2018. Middle and late Badenian palaeoenvironments in the northern Vienna Basin and their potential link to the Badenian Salinity Crisis. Geol. Carpath. 69, 149–168. https://doi.org/10.1515/geoca-2018-0009.

Hsü, K.J., Giovanoli, F., 1979. Messinian event in the black sea. Palaeogeogr. Palaeoclimatol. Palaeoecol. 29, 75–93. https://doi.org/10.1016/0031-0182(79)90075-0.

İslamoğlu, Y., Harzhauser, M., Gross, M., Jiménez-Moreno, G., Ćorić, S., Kroh, A., Rögl, F., van der Made, J., 2008. From Tethys to Eastern Paratethys: Oligocene depositional environments, paleoecology and paleobiogeography of the Thrace Basin (NW Turkey). Int J Earth Sci (Geol Rundsch) 99, 183–200. https://doi.org/10.1007/s00531-008-0378-0.

Jones, R.W.W., Simmons, M.D., 1997. A review of the stratigraphy of eastern Paratethys (Oligocene-Holocene), with particular emphasis on the Black Sea. Reg. Pet. Geol. Black Sea Surround. Reg. AAPG Mem. 68, 39–52.

Jørgensen, B.B., 1982. Mineralization of organic matter in the sea bed—the role of sulphate reduction. Nature 296, 643–645. https://doi.org/10.1038/296643a0.

Kaya MY, Dupont-Nivet G, Proust JN, Roperch P, Bougeois L, Meijer N, 2019. Paleogene evolution and demise of the proto-Paratethys Sea in Central Asia (Tarim and Tajik basins): Role of intensified tectonic activity at ca. 41 Ma. vol. 31. doi:https://doi.org/10.1111/bre.12330.

Kováč, M., Andreyeva-Grigorovich, A., Bajraktarević, Z., Brzobohatý, R., Filipescu, S., Fodor, L., 2007. Badenian evolution of the Central Paratethys Sea: Paleogeography, climate and eustatic sea-level changes. Geol. Carpath. 58, 579–606.

Kováč, M., Hudáčková, N., Halásová, E., Kováčová, M., Holcová, K., Oszczypko-Clowes, M., 2017. The Central Paratethys palaeoceanography: a water circulation model based on microfossil proxies, climate and changes of depositional environment. Acta Geol Slovaca 9, 75–114.

Krijgsman, W., Stoica, M., Vasiliev, I., Popov, V.V., 2010. Rise and fall of the Paratethys Sea during the Messinian Salinity Crisis. Earth Planet. Sci. Lett. 290, 183–191. https://doi.org/10.1016/j.epsl.2009.12.020.

Krijgsman, W., Palcu, D.V., Andreetto, F., Stoica, M., Mandic, O., 2020a. Changing seas in the late Miocene Northern Aegean: a Paratethyan approach to Mediterranean basin evolution. Earth-Sci. Rev. 210, 103386. https://doi.org/10.1016/j.earscirev.2020.103386.

Krijgsman, W., Stoica, M., Hoyle, T.M., Jorissen, E.L., Lazarev, S., Rausch, L., Bista, D., Alçiçek, M.C., Ilgar, A., van den Hoek Ostende, L.W., Mayda, S., Raffi, I., Flecker, R., Mandic, O., Neubauer, T.A., Wesselingh, F., 2020b. The myth of the Messinian Dardanelles: late Miocene stratigraphy and palaeogeography of the ancient Aegean-Black Sea gateway. Palaeogeogr. Palaeoclimatol. Palaeoecol. 560. https://doi.org/10.1016/j.palaeo.2020.110033.

Krijgsman, W., Rohling, E.J., Palcu, D.V., Raad, F., Amarathunga, U., Flecker, R., Florindo, F., Roberts, A.P., Sierro, F.J., Aloisi, G., 2024. Causes and consequences of the Messinian salinity crisis. Nat Rev Earth Environ 5, 335–350. https://doi.org/10.1038/s43017-024-00533-1.

Lazarev, S., de Leeuw, A., Stoica, M., Mandic, O., van Baak, C.G.C., Vasiliev, I., 2020. From Khersonian drying to Pontian "flooding": late Miocene stratigraphy and palaeoenvironmental evolution of the Dacian Basin (Eastern Paratethys). Glob. Planet. Chang. 192, 103224. https://doi.org/10.1016/j.gloplacha.2020.103224.

Lazarev, S., Mandic, O., Stoica, M., Goldin, P., Ćorić, S., Harzhauser, M., 2025. Hydrological isolation of the Paratethys in the late Middle-late Miocene: Integrated stratigraphy, palaeoenvironments and biotic record of the Caspian Basin, Karagiye. Kazakhstan. Mar Pet Geol 173, 107288. https://doi.org/10.1016/j.marpetgeo.2025.107288.

Liu, Z., Algeo, T.J., Arefifard, S., Wei, W., Brett, C., Landing, E., Lev, S.M., 2024. Testing the salinity of Cambrian to Silurian epicratonic seas. J. Geol. Soc. Lond. 181 (3), 1–19 jgs2023-217.

Liu, Z., Algeo, T.J., Brocks, J.J., van Maldegem, L.M., Gilleaudeau, G.J., Kah, L.C., Cheng, M., Yu, W.C., 2025. Salinity reconstruction in Proterozoic depositional systems. Geol. Soc. Am. Bull. 447–464. https://doi.org/10.1130/b37489.1.

Liu, S., Krijgsman, W., Dekkers, M.J., Palcu, D.V., 2017. Early diagenetic greigite as an indicator of paleosalinity changes in the middle Miocene Paratethys Sea of central Europe. Geochemistry, Geophys. Geosystems 18, 2634–2645. https://doi.org/10.1002/2017GC006988.

McLennan, S.M., 2001. Relationships between the trace element composition of sedimentary rocks and upper continental crust. Geochem. Geophys. Geosyst. 2. https://doi.org/10.1029/2000GC000109, 2000GC000109.

Munteanu, I., Matenco, L., Dinu, C., Cloetingh, S., 2012. Effects of large sea-level variations in connected basins: the Dacian-Black Sea system of the Eastern Paratethys. Basin Res. 24, 583–597. https://doi.org/10.1111/j.1365-2117.2012.00541.x.

Musatov, V.A., Bogachkin, A.B., 2019. Bartonian stage of the Middle Eocene within European part of Russia. Stratigraphic Interval and Boundary Determination Criteria Article 2. Detailed Zonal Stratigraphy of the Lutetian-Barton Interval on Nannoplankton and Paleomagnetic Characteristics of Ci. Стратиграфия И Литология Удк 99, 3–34.

Nevesskaya, L.A., Goncharova, I.A., Iljina, L.B., Paramonova, N.P., Popov, S.V., Babak, E.V., 1986. History of Neogene mollusks of the Paratethys. Trans Paleontol Institute, Acad Sci USSR 220, 1–206.

Nevesskaya, L.A., Paramonova, N.P., Babak, E.V., 1997. Classification of Pliocene bivalves of Southwest Eurasia. Tr Paleontol Inst 269, 1–267.

Nevesskaya, L.A., Paramonova, N.P., Popov, S.V., 2001. History of lymnocardiinae (bivalvia, cardiidae). Paleontol. J. 35.

Nevesskaya, L.A., Gontsharova, I.A., Iljina, L.B., 2005. Types of Neogene marine and nonmarine basins exemplified by the Eastern Paratethys. Paleontol. Zh. 39, 10–12.

Okay, A.I., Topuz, G., Kylander-Clark, A.R.C., Sherlock, S., Zattin, M., 2022. Late Paleocene–Middle Eocene magmatic flare-up in western Anatolia. Lithos 428, 106816.

Palcu, D.V., Krijgsman, W., 2023. The dire straits of Paratethys: Gateways to the anoxic giant of Eurasia. Geol. Soc. London Spec. Publ. 523. https://doi.org/10.1144/SP523-2021-73. SP523–573.

Palcu, D.V., Tulbure, M., Bartol, M., Kouwenhoven, T.J., Krijgsman, W., 2015. The Badenian/Sarmatian extinction event in the Carpathian foredeep basin of Romania: Paleogeographic changes in the Paratethys domain. Glob. Planet. Chang. 133, 346–358. https://doi.org/10.1016/j.gloplacha.2015.08.014.

Palcu, D.V., Golovina, L.A., Vernyhorova, Y.V., Popov, S.V., Krijgsman, W., 2017. Middle Miocene paleoenvironmental crises in Central Eurasia caused by changes in marine gateway configuration. Glob. Planet. Chang. 158, 57–71. https://doi.org/10.1016/j.gloplacha.2017.09.013.

Palcu, D.V., Popov, S.V., Golovina, L.A., Kuiper, K.F., Liu, S., Krijgsman, W., 2019a. The shutdown of an anoxic giant: Magnetostratigraphic dating of the end of the Maikop Sea. Gondwana Res. 67, 82–100. https://doi.org/10.1016/j.gr.2018.09.011.

Palcu, D.V., Vasiliev, I., Stoica, M., Krijgsman, W., 2019b. The end of the Great Khersonian Drying of Eurasia: Magnetostratigraphic dating of the Maeotian transgression in the Eastern Paratethys. Basin Res. 31, 33–58. https://doi.org/10.1111/bre.12307.

Palcu, D.V., Patina, I.S., Şandric, I., Lazarev, S., Vasiliev, I., Stoica, M., 2021. Late Miocene megalake regressions in Eurasia. Sci. Rep. 11, 11471. https://doi.org/10.1038/s41598-021-91001-z.

Palcu, D.V., Mariş, I., de Leeuw, A., Melinte-Dobrinescu, M., Anton, E., Frunzescu, D., 2023. The legacy of the Tethys Ocean: Anoxic seas, evaporitic basins and megalakes in the Cenozoic of Central Europe. Earth-Sci. Rev. 246, 104594. https://doi.org/10.1016/j.earscirev.2023.104594.

Palmer, M.R., Edmond, J.M., 1989. The strontium isotope budget of the modern ocean. Earth Planet. Sci. Lett. 92, 11–26. https://doi.org/10.1016/0012-821X(89)90017-4.

Piller, W.E., Harzhauser, M., Mandić, O., 2007. Miocene Central Paratethys stratigraphy – current status and future directions. Stratigraphy 4, 151–168.

Poisson, A., Vrielynck, B., Wernli, R., Negri, A., Bassetti, M.A., Büyükmeriç, Y., Özer, S., Guillou, H., Kavak, K.S., Temiz, H., Orszag-Sperber, F., 2016. Miocene transgression in the central and eastern parts of the Sivas Basin (Central Anatolia, Turkey) and the Cenozoic palaeogeographical evolution. Int J Earth Sci (Geol Rundsch) 105, 339–368. https://doi.org/10.1007/s00531-015-1248-1.

Popov, S.V., Studencka, B., 2015. Brackish-water Solenovian mollusks from the lower Oligocene of the Polish Carpathians. Paleontol. J. 49, 342–355. https://doi.org/10.1134/S0031030115040140.

Popov, S.V., Zastrozhnov, A., 1998. Neogene key sections of the Eastern Paratethys (Taman Peninsula). Tour Guid Volgogr 20.

Popov, S.V., Voronina, A.A., Goncharova, I.A., 1993. Stratigraphy and bivalves of the Lower Miocene of the Eastern Paratethys (in Russian), 256.

Popov, S.V., Rögl, F., Rozanov, A.Y., Steininger, F.F., Shcherba, I.G., Kováč, M., 2004. Lithological-paleogeographic maps of paratethys. CFS Cour Forschungsinstitut Senckenb 1–46.

Popov, S.V., Sychevskaya, E.K., Akhmet, M.A., Zaporozhets, N.I., Golovina, L.A., Akhmetiev, M.A., 2008. Stratigraphy of the Maikop Group and Pteropoda Beds in northern Azerbaijan. Stratigr. Geol. Correl. 16, 664–677. https://doi.org/10.1134/S0869593808060063.

Popov, S.V., Antipov, M.P., Zastrozhnov, A.S., Kurina, E.E., Pinchuk, T.N., 2010. Sea-level fluctuations on the northern shelf of the Eastern Paratethys in the Oligocene-Neogene. Stratigr. Geol. Correl. 18, 200–224. https://doi.org/10.1134/s0869593810020073.

Popov, S.V., Rostovtseva, Y.V., Fillippova, N.Y., Golovina, L.A., Radionova, E.P., Goncharova, I.A., 2016. Paleontology and stratigraphy of the Middle–Upper Miocene of the Taman Peninsula: Part 1. Description of key sections and benthic fossil groups. Paleontol. J. 50, 1039–1206. https://doi.org/10.1134/S0031030116100014.

Popov, S.V., Rostovtseva, Y.V., Pinchuk, T.N., Patina, I.S., Goncharova, I.A., 2019a. Oligocene to Neogene paleogeography and depositional environments of the Euxinian part of Paratethys in Crimean – Caucasian junction. Mar. Pet. Geol. 103, 163–175. https://doi.org/10.1016/j.marpetgeo.2019.02.019.

Popov, S.V., Tabachnikova, I.P., Bannikov, A.F., Sytchevskaya, E.K., Pinchuk, T.N., Akhmetiev, M.A., 2019b. Lectostratotype of the Maikopian Group in the Belaya River section upstream of the town of Maikop (Western Ciscaucasia) in the Oligocene part. Stratigr. Geol. Correl. 27, 339–360. https://doi.org/10.1134/S0869593819030043.

Popov, S.V., Tabachnikova, I.P., Pinchuk, T.N., Akhmetiev, M.A., Zaporozhets, N.I., 2019c. The reference section of Eocene deposits in the Belaya River Valley, Adygea, Western Ciscaucasia. Stratigr. Geol. Correl. 27, 118–132. https://doi.org/10.1134/S0869593819010052.

Popov, S.V., Golovina, L.A., Palcu, D.V., Goncharova, I.A., Pinchuk, T.N., Rostovtseva, Y.V., 2022. Neogene regional scale of the Eastern Paratethys, stratigraphy and paleontological basis. Paleontol. J. 56, 1557–1720. https://doi.org/10.1134/S0031030122120024.

Popov, S.V., Golovina, L.A., Palcu, D.V., Goncharova, I.A., Pinchuk, T.N., Rostovtseva, Y.V., 2023. Neogene of the Eastern Paratethys: a regional stage scale, reference sections and problems of correlation. Proc PIN RAS 299.

Radionova, E.P., Golovina, L.A., 2010. Late Miocene Events of the Black Sea Region: Comparative Study of Diatoms and Nannofossils from Sites 380, 381 DSDP Leg 42B

and Zheleznyi rog Section. XIX Congr. Carpathian Balk. Geol. Assoc., Thessaloniki, Greece, Taman Peninsula, p. 5.
Radionova, E.P., Golovina, L.A., 2011. Upper Maeotian-lower Pontian "Transitional Strata" in the Taman Peninsula: stratigraphic position and paleogeographic interpretation. Geol. Carpath. 62, 77–90. https://doi.org/10.2478/v10096-011-0007-x.
Radionova, E.P., Golovina, L.A., Filippova, N.Y., Trubikhin, V.M., Popov, S.V., Goncharova, I.A., 2012. Middle-Upper Miocene stratigraphy of the Taman Peninsula, Eastern Paratethys. Cent. Eur. J. Geosci. 4, 188–204. https://doi.org/10.2478/s13533-011-0065-8.
Raffi, I., Wade, B.S., Pälike, H., Beu, A.G., Cooper, R., Crundwell, M.P., 2020. In: Gradstein, F.M., Ogg, J.G., Schmitz, M.D., Ogg, G.M. (Eds.), Chapter 29 - The Neogene Period. Elsevier, pp. 1141–1215. https://doi.org/10.1016/B978-0-12-824360-2.00029-2.
Rögl, F., 1999. Palaeogeographic considerations for Mediterranean and Paratethys seaways (Oligocene to Miocene). Ann Natl Mus Wien, Ser A 101, 279–310.
Rögl, F., Steininger, F.F., 1983. Vom Zerfall der Tethys zur Paratethys. Ann. Naturhist. Mus. Wien 85, 135–163.
Rostovtseva, Y.V., Rybkina, A.I., 2017. The Messinian event in the Paratethys: Astronomical tuning of the Black Sea Pontian. Mar. Pet. Geol. 80, 321–332. https://doi.org/10.1016/j.marpetgeo.2016.12.005.
Roveri, M., Flecker, R., Krijgsman, W., Lofi, J., Lugli, S., Manzi, V., Sierro, F.J., Bertini, A., Camerlenghi, A., De Lange, G., Govers, R., Hilgen, F.J., Hübscher, C., Meijer, P.T., Stoica, M., 2014. The Messinian Salinity Crisis: past and future of a great challenge for marine sciences. Mar. Geol. 352, 25–58. https://doi.org/10.1016/j.margeo.2014.02.002.
Rybkina, A.I., Rostovtseva, Y.V., 2014. Astronomically-tuned cyclicity in Upper Maeotian deposits of the Eastern Paratethys (Zheleznyi Rog section, Taman). Mosc. Univ. Geol. Bull. 69, 341–346. https://doi.org/10.3103/s0145875214050081.
Rybkina, A.I., Kern, A.K., Rostovtseva, Y.V., 2015. New evidence of the age of the lower Maeotian substage of the Eastern Paratethys based on astronomical cycles. Sediment. Geol. 330, 122–131. https://doi.org/10.1016/j.sedgeo.2015.10.003.
Sachsenhofer, R.F., Gratzer, R., Bechtel, A., Gusterhuber, J., Ćorić, S., Harzhauser, M., Piller, W.E., Mayer, J., Reischenbacher, D., Schmid, C., Stanzer, A., Gross, D., 2016. Oligocene–Miocene source rocks in the Paratethys: Early Oligocene Maikop Group productivity and Solenovian Event implications. AAPG Bull. 101, 289–317. https://doi.org/10.1306/04151615198.
Sachsenhofer, R.F., Popov, S.V., Akhmetiev, M.A., Bechtel, A., Gratzer, R., Groß, D., 2017. The type section of the Maikop Group (Oligocene-lower Miocene) at the Belaya River (North Caucasus): Depositional environment and hydrocarbon potential. Am. Assoc. Pet. Geol. Bull. 101, 289–319. https://doi.org/10.1306/08051616027.
Sachsenhofer, R.F., Popov, S.V., Čorić, S., Mayer, J., Misch, D., Morton, M.T., Pupp, M., Rauball, A., Tari, G., 2018. Paratethyan petroleum source rocks: an overview. J. Pet. Geol. 41, 219–245. https://doi.org/10.1111/jpg.12702.
Sant, K., Palcu, D.V., Mandic, O., Krijgsman, W., 2017. Changing seas in the Early-Middle Miocene of Central Europe : a Mediterranean approach to Paratethyan stratigraphy. Terra Nova 29, 273–281. https://doi.org/10.1111/ter.12273.
Sant, K., Palcu, D.V., Turco, E., Di Stefano, A., Baldassini, N., Kouwenhoven, T., 2019a. The mid-Langhian flooding in the eastern Central Paratethys: integrated stratigraphic data from the Transylvanian Basin and SE Carpathian Foredeep. Int. J. Earth Sci. 108, 2209–2232. https://doi.org/10.1007/s00531-019-01757-z.
Sant, K., Palcu, D.V., Turco, E., Di Stefano, A., Baldassini, N., Kouwenhoven, T., 2019b. Litho- and biostratigraphic data of lower-middle Miocene sections in the Transylvanian basin and SE Carpathian Foredeep (Romania). Data Br 24, 103904. https://doi.org/10.1016/j.dib.2019.103904.
Schleiffarth, W.K., Darin, M.H., Reid, M.R., Umhoefer, P.J., 2018. Dynamics of episodic Late Cretaceous–Cenozoic magmatism across Central to Eastern Anatolia: New insights from an extensive geochronology compilation. Geosphere 14, 1990–2008. https://doi.org/10.1130/GES01647.1.
Schmid, S.M., Bernoulli, D., Fügenschuh, B., Matenco, L., Schefer, S., Schuster, R., 2008. The Alpine-Carpathian-Dinaridic orogenic system: Correlation and evolution of tectonic units. Swiss J. Geosci. 101, 139–183. https://doi.org/10.1007/s00015-008-1247-3.
Schulz, H.M., Bechtel, A., Sachsenhofer, R.F., 2005. The birth of the Paratethys during the early Oligocene: from Tethys to an ancient Black Sea analogue? Glob. Planet. Chang. 49, 163–176. https://doi.org/10.1016/j.gloplacha.2005.07.001.
Simon, D., Palcu, D.V., Meijer, P., Krijgsman, W., 2019. The sensitivity of middle Miocene paleoenvironments to changing marine gateways in Central Europe. Geology 47, 35–38. https://doi.org/10.1130/G45698.1.
Soták, J., 2010. Paleoenvironmental changes across the Eocene-Oligocene boundary: Insights from the Central-Carpathian Paleogene Basin. Geol. Carpath. 61, 393–418. https://doi.org/10.2478/v10096-010-0024-1.
Stoica, M., Krijgsman, W., Fortuin, A., Gliozzi, E., 2016. Paratethyan ostracods in the Spanish Lago-Mare: more evidence for interbasinal exchange at high Mediterranean Sea level. Palaeogeogr. Palaeoclimatol. Palaeoecol. 441, 854–870. https://doi.org/10.1016/j.palaeo.2015.10.034.
Speijer, R.P., Pälike, H., Hollis, C.J., Hooker, J.J., Ogg, J.G., 2020. Chapter 28 - The Paleogene Period. In: Gradstein, F.M., Ogg, James G, Schmitz, M.D., Ogg, G.M. (Eds.), Geologic Time Scale 2020. Elsevier, pp. 1087–1140. https://doi.org/10.1016/B978-0-12-824360-2.00028-0.
Studencka, B., Jasionowski, M., 2011. Bivalves from the Middle Miocene reefs of Poland and Ukraine: a new approach to Badenian/Sarmatian boundary in the Paratethys. Acta Geol. Pol. 61, 79–114.
Tribovillard, N., Algeo, T.J., Lyons, T., Riboulleau, A., 2006. Trace metals as paleoredox and paleoproductivity proxies: an update. Chem. Geol. 232, 12–32. https://doi.org/10.1016/j.chemgeo.2006.02.012.
Tulan, E., Sachsenhofer, R.F., Tari, G., Flecker, R., Fairbank, V., Pupp, M., Gratzer, R., Bechtel, A., Čorić, S., Linzer, H.G., 2020. Source rock potential and depositional environment of the lower Oligocene İhsaniye Formation in NW Turkey (Thrace, Karaburun). Turk. J. Earth Sci. 29, 64–84. https://doi.org/10.3906/yer-1906-14.
van Baak, C.G.C.C., Stoica, M., Grothe, A., Aliyeva, E., Krijgsman, W., 2016. Mediterranean-Paratethys connectivity during the Messinian salinity crisis: the Pontian of Azerbaijan. Glob. Planet. Chang. 141, 63–81. https://doi.org/10.1016/j.gloplacha.2016.04.005.
van Baak, C.G.C., Krijgsman, W., Magyar, I., Sztanó, O., Golovina, L.A., Grothe, A., et al., 2017. Paratethys response to the Messinian salinity crisis. Earth-Sci. Rev. 172, 193–223. https://doi.org/10.1016/j.earscirev.2017.07.015.
van der Boon, A., van der Ploeg, R., Cramwinckel, M.J., Kuiper, K.F., Popov, S.V., Tabachnikova, I.P., 2019. Integrated stratigraphy of the Eocene-Oligocene deposits of the northern Caucasus (Belaya River, Russia): Intermittent oxygen-depleted episodes in the Peri-Tethys and Paratethys. Palaeogeogr. Palaeoclimatol. Palaeoecol. 536, 109395. https://doi.org/10.1016/j.palaeo.2019.109395.
van der Boon, A., Kuiper, K.F., van der Ploeg, R., Cramwinckel, M.J., Honarmand, M., Sluijs, A., 2021. Exploring a link between the Middle Eocene Climatic Optimum and Neotethys continental arc flare-up. Clim. Past 17, 229–239. https://doi.org/10.5194/cp-17-229-2021.
Vasiliev, I., Iosifidi, A.G., Khramov, A.N., Krijgsman, W., Kuiper, K., Langereis, C.G., 2011. Magnetostratigraphy and radio-isotope dating of upper Miocene-lower Pliocene sedimentary successions of the Black Sea Basin (Taman Peninsula, Russia). Palaeogeogr. Palaeoclimatol. Palaeoecol. 310, 163–175. https://doi.org/10.1016/j.palaeo.2011.06.022.
Vincent, S.J., Morton, A.C., Carter, A., Gibbs, S., Barabadze, T.G., 2007 Apr. Oligocene uplift of the Western Greater Caucasus: an effect of initial Arabia–Eurasia collision. Terra Nova 19 (2), 160–166.
Wei, W., Algeo, T.J., 2020. Elemental proxies for paleosalinity analysis of ancient shales and mudrocks. Geochim. Cosmochim. Acta 287, 341–366. https://doi.org/10.1016/j.gca.2019.06.034.
Wei, W., Algeo, T.J., Meyer, D., Liu, J.S., Snihur, K.N., Lazowski, C., Li, Z.Q., Alessi, D.S., Konhauser, K.O., Du, Y.S., Yu, W.C., 2025. Utility of the B/Ga salinity proxy in carbonate and marly sediments. Chem. Geol. 682, 122751.
Zaporozhets, N.I., 1999. Palynostratigraphy and dinocyst zonation of the middle Eocene-lower Miocene deposits at the Belaya River (Northern Caucasus). Stratigr. Geol. Correl. 7, 161–178.
Zhang, J., Wei, W., Wie, X., Krijgsman, W., Feng, Y., Li, Y., Cao, W., Ma, Y., Yang, H., Zhang, Y., Li, H., Xia, W., Liu, Y., Liu, Q., 2025. Salinity and hydrology reconstructions using B/Ga proxy records in the Pearl River Estuary (China). Chem. Geol. 685, 122809. https://doi.org/10.1016/j.chemgeo.2025.122809.